Study on Noise Suppression Mechanism of Magnetic Film for On-Chip Design

Ph. D Thesis

Study on Noise Suppression Mechanism of Magnetic Film for On-Chip Design

オンチップ設計に向けた磁性膜によるノイズ抑制機構に関する研究

Jingyan Ma

Department of Electrical Engineering

Graduate School of Engineering

TOHOKU UNIVERSITY

2018

ABSTRACT

In this thesis, three types of magnetic films with different permeabilities and resistivities are studied in terms of magnetic shielding effectiveness, conductive noise suppression, and crosstalk. The experiment is based on a proposed method, which involves microstrip lines covered by magnetic films. The results of magnetic shielding effectiveness, conductive loss, and crosstalk obtained for both measurement and simulation are in agreement.

Based on the variability of the simulator, the contributions of permeability and resistivity are separately confirmed. The results show that the frequency of maximum shielding corresponds to the ferromagnetic resonance (FMR) frequency of the magnetic film, while permeance and sheet resistance dominates the value of the shielding effect at FMR frequency. Doubling the value of permeability or halving resistivity leads to the improvement of the maximum shielding effect by about 3 dB.

Conversely, the crosstalk suppression brought about by the magnetic film was confirmed. The crosstalk suppression at a particular frequency can be attributed to ferromagnetic resonance. In addition, the distribution of magnetic flux density inside the magnetic film when placed on a microstrip line is clarified by formula calculation and simulation. This may help the quantitative study of crosstalk influence and equivalent circuit analysis.

The proposed study will boost development related to the mechanism study of magnetic film-type noise suppressors. Moreover, it can support the design guidelines of magnetic film-type noise suppressors used in next generation IC chips.

CONTENTS

LIST OF FIGURES

LIST OF TABLES

Chapter 1
Introduction

1.1 Overview

The world of Internet of Things (IoT) is experiencing an explosive phenomenon with more than 75 million devices predicted to join in the IoT team by 2025 [1].

IoT is defined as the network of physical items that is growing rapidly based on the development of internet, electronics, sensors, and other technologies. The challenges that IoT faces include data managing, connection reliability, data security etc. [2]. Among these, as with the new definition of More than Moore [3], integrated circuits (ICs) of electrical devices are required to possess high-speed data processing, low power consumption, high integration, and multifunctionality. The transistors with smaller gate lengths in RF/mixed-signal system-on-chips (SoCs) lead to increased integration and thus higher efficiency [4]. For example the frequency band of a telecommunication system grows from 900 MHz (2^{nd} generation GSM) to 2600 MHz (4^{th} generation 3GPP), which portrays an urgent demand in the transmission capacity. High integration, broad bandwidth, and high operating frequency are required in the future development of IC chips.

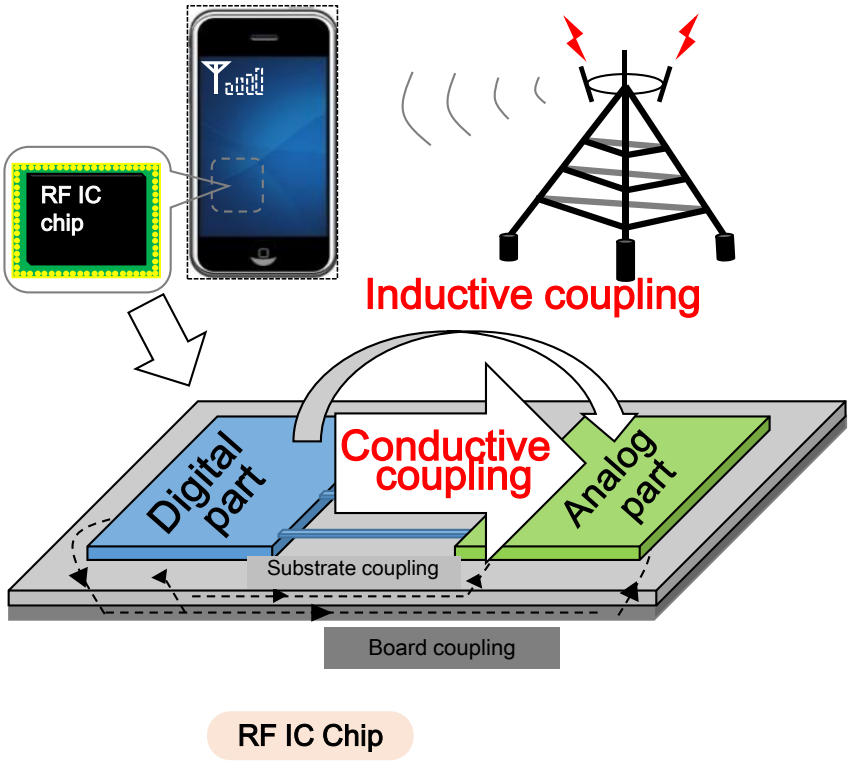

Fig. 1.1 Inductive and conductive noise coupling in an RF IC chip

However, this next generation technologies will certainly hamper the safety of electromagnetic interference (EMI) of IC chips. The high order harmonics from multiple clock frequencies in digital circuits interfere with the signal sensitivity of analog circuits' receiver circuit chain. Additionally, the near field electromagnetic emission should be carefully considered in the 3D IC chip package design [4][5]. As shown in Fig. 1.1., inductive and conductive couplings between the digital circuit and analog circuit parts are serious problems. Therefore, countermeasures are critically necessary.

The narrow gate length of transistors was improved to less than 10 nm in 2017 and is expected to decrease further in the future [73]. In the standard of IMT-2020, the throughput of 5^{th} G exceeds 10 Gbps per connection, which is 100 times that of the 4^{th} G [7][64]. Therefore, with future improvements, systems possessing finer CMOS technology, closer distances, and varying clock frequencies to maintain vast baseband digital signal processing will increase, thereby causing a potentially serious problem with the failure of signal receiving and transfer [8]-[10].

Inductive coupling generated by magnetic flux, along with resistive and capacitive coupling generated by conduction and displacement currents are seriously affecting the electromagnetic compatibility of IC chips.

There are three types of noise coupling paths in an IC chip: inductive coupling, capacitive coupling, and resistive coupling. The inductive coupling is based on magnetic flux, which is generated from currents and radiates throughout the surrounding space. Resistive coupling is based on conduction current and generated through the silicon substrate. Capacitive coupling is based on displacement current, which is generated between adjacent conductors. Both resistive and capacitive coupling mainly belong to substrate coupling. They are studied by electromagnetic compatibility (EMC) models

experiments and simulations [11]-[13].

The countermeasures for such electromagnetic interferences are described as follows [14]-[20],

(1) circuit technologies, such as clock frequency selection for harmonics management,

(2) layout design technologies, such as IPs, wire routing, and metallic guard bands,

(3) physical process technologies, such as SOI, triple-well, and high-resistivity substrate,

(4) device technologies, such as shielding-type cover, filter.

Among them, the shielding-type cover with a noise suppression function without increasing any footprints on the chip compared to the layout design is proposed. It is beneficial to apply it without increasing the plane area of the chip as it can provide appropriate magnetic shielding and electromagnetic wave absorption. Furthermore, the shielding-type covers have the advantages of lightweight, flexibility [47], and high strength [70], and these properties are required in high-density ICs as well. However, the high requirements of fabrication quality makes it has a high cost and complex machining process especially for carbon based shielding-type covers [71], and additionally the material source is limited in the aspect of metal based shielding-type covers. These difficulties need to be overcome for commercial application of shielding-type cover.

1.2 Shielding-type noise suppressor

The shielding-type noise suppressors with different materials and structures are widely studied in ultra/super high frequency range, from 0.1 GHz to 30 GHz, as shown in Fig. 1.3. (1) Magnetic based, synthetic fiber, multi-walled carbon nanotube (MWCNT) [21]-[25] et al. are mainly applied in L, S, and C bands that are occupied for mobile and

wireless communications (such as 4th and 5th generation and blue tooth tech.). (2) MXenes, reduced graphene oxide (rGO) based material, and graphite [26]-[31] are mainly applied in X and Ku bands that are occupied by radar and meteorological satellites. (3) Graphene, pyrolytic carbon [32][33] et al. are mainly applied in K and Ka bands that are occupied by communication satellites. Detailed information related to several shielding-type noise suppressors is listed in Table 1. There are mainly seven types of shielding-type noise suppressors with different materials that can provide magnetic shielding and/or absorption effects.

(1) Graphene and rGO, which are fabricated as 2-dimension structures based on carbon atoms, are attracting great attention in the field of EMI shielding. Most graphene and rGO films are applied in the X band, which is 8.2–12.4 GHz wide. Graphene is reported to be thinner (μm) than rGO (mm) and has a certain characteristics of wave absorption. rGO provides good EMI shielding with its great wave absorption capability.

(2) Graphite has been used for EMI shielding since the 1990s owing to its good resistance to corrosion, low-cost, and easy fabrication. It has a wide range of applications in the frequencies from MHz to GHz. Graphite is more simple than graphene and has a better design freedom, whereas its thickness (~ mm) is considered as an obstacle for future EMI works on IC chips.

(3) Carbon nanotube and carbon fibers are mainly used in the X band, and have thicknesses lesser than 5 mm. Compared to the metal, they have better electrical and mechanical properties such as high conductivity, flexibility, and lightweight. Among them, H. M. Kim's MWCNT/PMMA is thinner than others (0.06–0.165 mm), and is applied in a lower frequency range (0.05–13.5 GHz) [47].

(4) MXene was studied first in 2011 [56] as a new graphene-like 2-D inorganic compounds, which has good conductivity and high capacitance. It has been reported early for use in energy storage devices [57] [58]. F. Shahzad [18] first investigated MXene-SA composites with regards to its EMI shielding property. This material possesses great EMI shielding effect with lower thickness (~ μm) compared to other shielding carbon materials.

(5) Metamaterials (MMs) that are used as shielding-type noise suppressors are based on different shapes/structures of copper, aiming to manipulate resonance in ε and μ. At the resonance frequency, the absorption of magnetic field is maximum. This kind of material is advantageous in having narrow absorption bands, controllable and multi-frequency bands. Although the average absorption efficiency is larger than that of magnetic films, it is affected by the incident angle of the waves. The thickness of metamaterials is not an advantage and the absorption wavelength is mainly decided by the size.

(6) Magnetic based materials are proposed with high permeability and conductivity. Most of them are anisotropic and soft magnets. They are reported to possess good EMI shielding as well as good wave absorption properties. They have a thickness of only a few microns. The details will be discussed in the next section.

1.3 Magnetic film-type noise suppressor

The magnetic material based films are proposed to be as follows,

(1) Thin/lightweight. The thickness of a fabricated magnetic film is only a few microns (including single-layered and multi-layered). The total thickness of magnetic film is thinner than most of the carbon materials mentioned above and conventional metals.

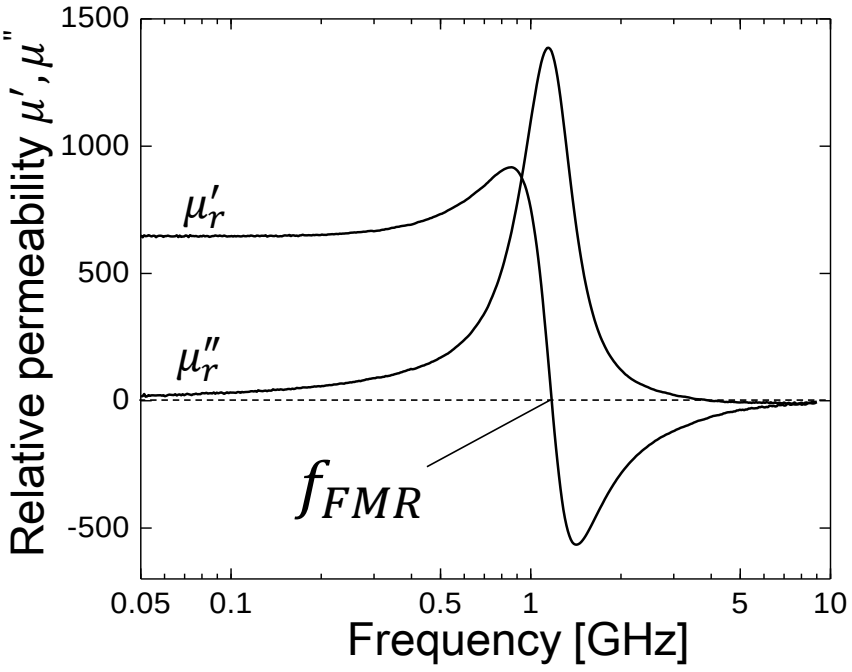

Fig. 1.2 Frequency dependence of relative permeability of a magnetic film

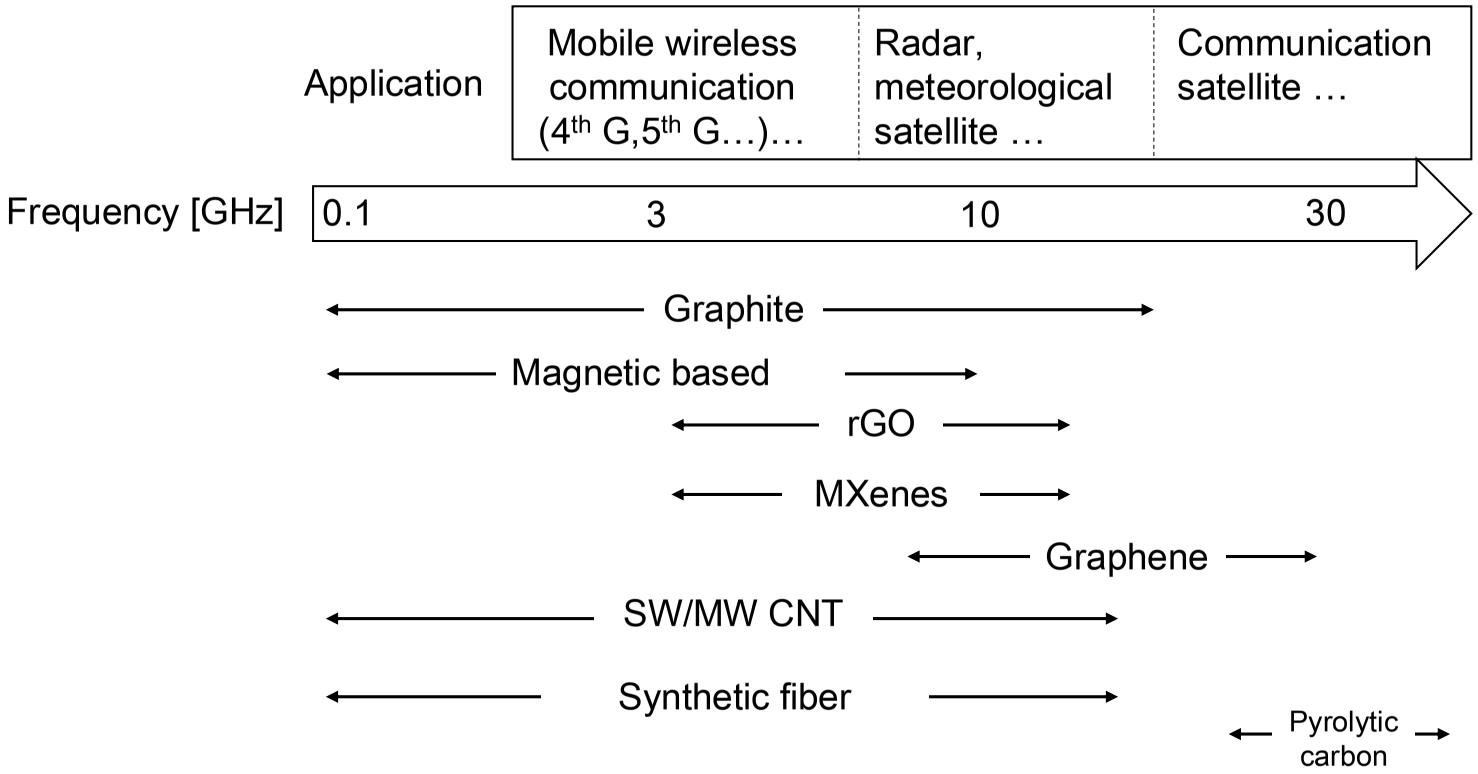

Fig. 1.3 Different types of shielding-type noise suppressors applied in different frequency bands

(2) Frequency-selective. The magnetic film has a complex frequency dependent relative permeability $\mu = \mu' - j\mu''$ as shown in Fig. 1.2. The imaginary part of the permeability causes magnetic loss with electrical wave absorption. In the frequency of ferromagnetic resonance (FMR), the real part of permeability μ' is zero and the imaginary part of permeability μ'' is at the peak. The magnetic loss is at the peak and thus could simultaneously provide highest EMI shielding and wave absorption at the FMR frequency. Different magnetic materials with different FMR frequencies are supposed to be applied in different IC chips with different operating frequencies. This property is fascinating and distinctive compared to other materials.

(3) Good magnetic shielding effect. Before FMR frequency, owing to high relative permeability, magnetic flux is concentrated inside the magnetic film and thus obtains a good EMI shielding effect.

(4) Good wave absorption. The high conductivity of the magnetic film leads to great eddy current loss, which converts the electrical energy into heat and dissipates it. As shown in table 1.1, except for the magnetic type, high wave absorptions occur in cases that have magnetic material fillers, which are potentially capable of wave absorption[40][50][52].

Except for the advantages mentioned above, magnetic films are not beneficial in terms of corrosion-resistance and flexibility.

In the aspect of chip application, two blocks of crossed-anisotropy multilayered Co-Zr-Nb magnetic films were deposited onto a LTE (long term evolution) - class wireless telecommunication RF IC (radio frequency integrated circuit) receiver test chip that had a carrier frequency of 2.1 GHz [59] as shown in Fig. 1.4 (a). The result is shown in Fig. 1.4 (b) that in the bandwidth of 5 MHz, the spurious (noise) was suppressed by more than

10 dB when the chip was covered by magnetic films. Meanwhile, the RF receiver-block of the chip operated normally even in the presence of the magnetic films, which shows that the magnetic films do not have side effect on the normal working of the chip. Furthermore, an improvement of minimum input power level to meet the 3GPP criteria by 8 dB are confirmed, which may help increase the signal sensitivity of the chip. Furthermore, owing to the high permeability of magnetic films, the magnetic near field radiation of magnetic film-covered chip was lower than the uncovered chips.

Then, the magnetic film was deposited as a patterned structure as shown in Fig. 1.4 (c), aiming to block the inductive/conductive noisy diffusion generated in the magnetic film. The patterned magnetic film was used to only cover possible aggressor and victim wires. As a result, a higher ratio of throughput and a lower in-band spurious tone was obtained compared to the former non-patterned magnetic film [60].

On the other hand, equivalent circuits were established based on the model of a microstrip line covered by a magnetic film [61]. The FMR property and eddy/displacement current (joule loss) were studied separately to explain the conductive noise suppression effect of magnetic films [62].

In the aspect of mechanism study, a model that was constructed by a group of signal and power lines similar to the test chip mentioned above was established to investigate the inductive couplings of the chip [63]. The results show that the main inductive coupling is related to the arbitrary noise generator, while the main conductive coupling is based on the lines. Therefore, the magnetic field radiation and crosstalk between lines must be considered in the design of film-type noise suppressors.

Table 1.1 Several shielding type noise suppressor

Type	Composite	Applied frequency (GHz)	Thickness (mm)	SE (dB)	Absorption (%)	Ref.
Graphene	/polymer	8 ~ 12	0.04~0.06	14	70%	[34]
	/Fe_3O_4	8 ~ 12	2.5	18.2	-	[35]
	/PMMA	30	4.2	-	54%	[32]
rGO	/polymer	8 ~ 12	2.5	45.1	-	[36]
	/γ-Fe_2O_3	8 ~ 12	-	45.26	-	[37]
	/SiO_2	8 ~ 12	1.5	37	-	[38]
	(Large area film)	1 ~ 4	0.015	20	-	[39]
	/$BaFe_{12}O_{19}$	12.4 ~ 18	3	32	99.8%	[40]
	/WPU	8 ~ 12	1	34	High	[41]
Graphite	/polyaniline	8 ~ 12	2	33.6	-	[42]
	/copper	1 ~ 20	2	50 ~ 70	High	[43]
	/ABS	0.03 ~ 1	3	60	High	[31]
CNT	/polystyrene	8 ~ 12	-	20	-	[44]
	SWCNT	0.01 ~ 1.5	1.5	20 (1GHz)	-	[45]
	SWCNT	8 ~ 12	2	30	-	[46]
	MWCNT /PMMA	0.05 ~ 13.5	0.06 ~ 0.165	27	High	[47]

	MWCNT /PTT	12.4 ~ 18	2	42	-	[48]
CF	/SiO_2	8 ~ 12	5	10	-	[49]
	/Ni/ABS	0.03 ~ 1	-	30	-	[50]
	/polypropyl-ene	8 ~ 12	3.2	25	-	[51]
	/Fe_3O_4	8 ~ 12	0.7	67.9	High	[52]
MXene	-	8 ~ 12	0.045	92	-	[18]
	-	11.6	1	76.1	-	[26]
Meta-materials	-	11.6	1.7	-	88%	[65]
	-	7.8-14.7	5	-	90%	[66]
	-	2.76	0.036	-	99.9%	[67]
	-	155.48	0.16	-	99.5%	[68]
	-	3-12*	4.905	-	80%	[69]
Magnetic type	CoZrNb	1	0.002	35	70%	[53]
	CoFe/AlN	1.7	0.0015	20	60%	[54]
	Fe-Si-Al /polymer	2	0.5	-	90%	[55]

* Only at the resonance points of frequency

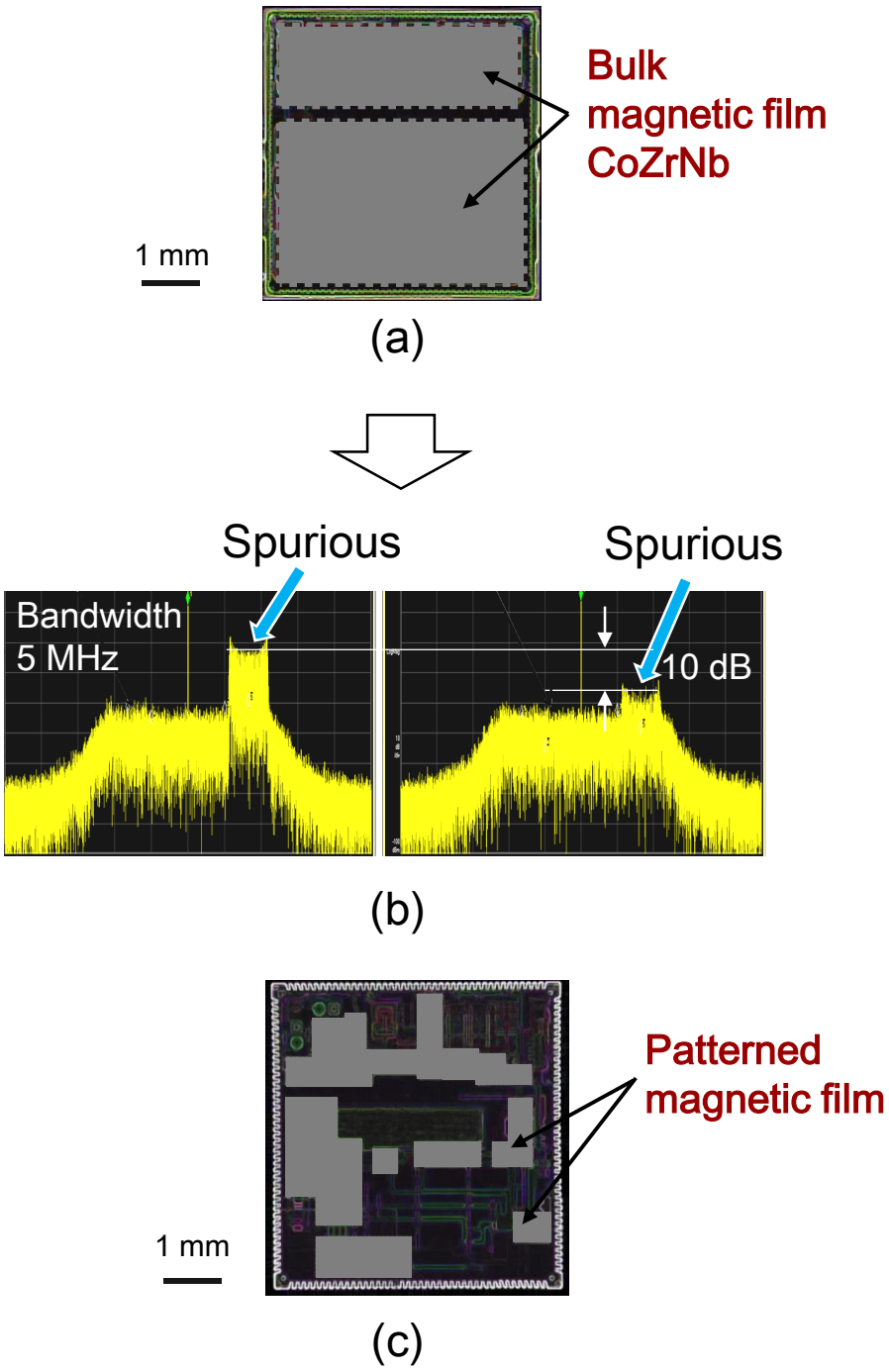

Fig. 1.4 (a) LTE test chip that is covered by two parts of magnetic film, and the spurious of film-covered chip is suppressed by 10 dB @ 2.1 GHz (LTE band 1) in the band of 5 MHz, (b) patterned magnetic film could provide a better noise suppression effect.

1.4 Objectives of this study

Firstly, although the magnetic film was applied to the LTE test chip and obtained good noise suppression as mentioned in 1.3, the mechanism investigation of permeability, resistivity, and the structure such as thickness and layers of magnetic film have not been totally clarified yet.

Since the magnetic film is effective in both inductive and conductive noise suppression when covered on the chip, the interaction between inductive and conductive couplings is important and needs to be confirmed.

Moreover, the couplings between lines as studied before play a significant role in crosstalk performance. The study of crosstalk between two signal lines when covered by magnetic film is expected.

The goal of this study is to complete the deficiencies mentioned above; firstly, to clarify the contribution of magnetic material's characteristics such as permeability, resistivity etc. Secondly, to discuss the interaction effect between the inductive and conductive noise suppression of magnetic films. Finally, to investigate the crosstalk performance between two parallel lines when they are covered by the magnetic film.

Therefore, in this study, the investigation of noise suppression mechanism of magnetic films will be continually processed. First, an experimental model will be established in order to evaluate inductive and conductive noise suppression simultaneously [53] [72], which occur at the same frequency spectrum. The relationship between inductive and conductive noise suppression along with the frequency will be confirmed. Second, the noise suppression effect of magnetic films with different materials will be measured and simulated; the contribution of permeability, resistivity, and dimension design to noise suppression will be clarified. Finally, the crosstalk performance of magnetic films will be

measured and simulated.

The next telecommunication generation is predicted to have a frequency band of 3.3 - 4.2 GHz [7] wherein the noise coupling issue will occur as well. Magnetic film is considered a prospective candidate to solve chip level noise coupling problems in higher frequency ranges. Thus, from the material point of view, the final objective is to support the design guidelines of the magnetic film-type noise suppressor used in next generation IC chips.

1.5 Outline

Chapter 1 introduces the background of the EMI situation, noise suppression methods, and shielding-type noise suppressors in recent years. The advantages and disadvantages of magnetic film-type noise suppressors are described in comparison to other material cases.

Chapter 2 proposes a method that can evaluate magnetic near-field shielding and conductive loss simultaneously. Both are dependent along with the frequency. The near-field shielding, conductive loss, and crosstalk of three types of magnetic films are measured.

Chapter 3 investigates the mechanism of magnetic films from the material point of view including FMR property and resistivity. The demagnetizing field that is generated inside the magnetic film, opposite in direction to the magnetic field outside, is considered the reason for maximum conductive loss. Furthermore, the demagnetizing factor is calculated to investigate the shifted FMR frequency. In this chapter, a similar model is established in a 3-dimension electromagnetic simulator, to study the noise suppression under different conditions.

Chapter 4 is based on the experimental results, investigating the mechanism of crosstalk of magnetic film by using the same electromagnetic simulation method. The magnetic flux density distribution inside the magnetic film is calculated and simulated, which is aimed at helping build an equivalent circuit to quantitatively study the inductive crosstalk influence when the magnetic film is covered on the chip.

Chapter 5 summarizes the whole work of this study and discusses the future outlook

References

[1] Sam Lucero. 2016. IoT platforms: enabling the Internet of Things. IHS Technology - Whitepaper (2016), 1-21

[2] IEEE International Roadmap for Devices and Systems, 2017 edition

[3] W. Arden, M. Brillouet, P. Cogez, M. Graef, B. Huizing, R. Mahnkopf, More than Moore White Paper by the IRC, Tech. Rep., International Technology Roadmap for Semiconductors, 2010

[4] Uemura, S., Hiraoka, Y., Kai, T., & Dosho, S. "Isolation techniques against substrate noise coupling utilizing through silicon via (TSV) process for RF/mixed-signal SoCs." IEEE Journal of Solid-State Circuits 47.4, 2012, pp. 810-816

[5] Lau, John H. "Overview and outlook of three-dimensional integrated circuit packaging, three-dimensional Si integration, and three-dimensional integrated circuit integration." Journal of Electronic Packaging 136.4, 2014, 040801

[6] Miettinen, J., Mantysalo, M., Kaija, K., & Ristolainen, E. O., “System design issues for 3D system-in-package (SiP),” Electronic Components and Technology Conference, Proceedings. 54th. IEEE, 2004. pp. 610-615

[7] Overview of ITU-T activities on 5G/IMT-2020, https://www.itu.int/

[8] C. Auth, C. Allen, A. Blattner, D. Bergstrom, M. Brazier, M. Bost, M. Buehler, V. Chikarmane, T. Ghani, T. Glassman, R. Grover, W. Han, D. Hanken, M. Hattendorf, P. Hentges, R. Heussner, J. Hicks, D. Ingerly, P. Jain, S. Jaloviar, R. James, D. Jones, J. Jopling, S. Joshi, C. Kenyon, H. Liu, R. McFadden, B. McIntyre, J. Neirynck, C. Parker, L. Pipes, I. Post, S. Pradhan, M. Prince, S. Ramey, T. Reynolds, J. Roesler, J. Sandford, J. Seiple, P. Smith, C. Thomas, D. Towner, T. Troeger, C. Weber, P. Yashar, K. Zawadzki, K. Mistry, “A 22nm high performance and low-power CMOS

technology featuring fully-depleted tri-gate transistors, self-aligned contacts and high density MIM capacitors," VLSI technology (VLSIT), 2012 symposium on. IEEE, 2012. pp. 131-132

[9] Razavi, Behzad, "Prospects of CMOS technology for high-speed optical communication circuits," IEEE Journal of Solid-State Circuits, 2002, 37.9, pp. 1135-1145

[10] LEE, Jri, "A 3-to-8-GHz fast-hopping frequency synthesizer in 0.18-/spl mu/m CMOS technology," IEEE Journal of Solid-State Circuits, 2006, 41.3, pp. 566-573

[11] Araga, Y., Nagata, M., Miura, N., Ikeda, H., & Kikuchi, K, "Measurement and Analysis of Power Noise Characteristics for EMI Awareness of Power Delivery Networks in 3-D Through-Silicon Via Integration," IEEE Transactions on Components, Packaging and Manufacturing Technology 8.2, 2018, pp. 277-285

[12] R Gharpurey, Robert G. Meyer, "Modeling and analysis of substrate coupling in integrated circuits," IEEE journal of solid-state circiuits, vol. 31, 1996, pp. 344-353

[13] M Yamaguchi, S Koya, H Torizuka, S Aoyama, S Kawahito, "Shield-loos-type on chip magnetic-field probe to evaluate radiated emission from thin-film noise suppressor," IEEE Trans. Magn. vol.43, no. 6, 2007, pp. 2370-2372

[14] J Kim, H Kim, W Ryu, J Kim, Y Yun, S Kim, S Ham, H An, Y Lee, "Effects of on-chip and off-chip decoupling capacitors on electromagnetic radiated emission," Electronic Components and Technology Conference, vol. 48, 1998, pp. 610-614

[15] Y Kayano, M Tanaka, J L Drewniak, H Inoue, "Common-mode current due to a trace near a PCB edge and its suppression by a guard band," IEEE Transactions on Electromagnetic compatibility, vol. 46, no. 1, 2004, pp. 46-53

[16] Okazaki, Y., Kobayashi, T., Konaka, S., Morimoto, T., Takahashi, M., Imai, K., &

Kado, Y., “Characteristics of a new isolated p-well structure using thin epitaxy over the buried layer and trench isolation,” IEEE Transactions on Electron Devices, vol. 39, no. 12, 1992, pp.2758-2764

[17] J Cho, E Song, K Yoon, J Pak, J Kim, W Lee, T Song, K Kim, J Lee, H Lee, K Park, S Yang, M Suh, K Byun, and J Kim, “Modeling and analysis of through-silicon via (TSV) noise coupling and suppression using a guard ring,” IEEE Transactions on Components, Packaging and Manufacturing Technology, 1, 2011, pp. 220-233

[18] Shahzad, F., Alhabeb, M., Hatter, C. B., Anasori, B., Hong, S. M., Koo, C. M., and Gogotsi, Y., “Electromagnetic interference shielding with 2D transition metal carbides (MXenes),” Science, 353, 2016, pp. 1137-1140

[19] K. Lee, H. Lee, H. Jung, J. Sim and H. Park, “A serpentine guard trace to reduce the far-end crosstalk voltage and the crosstalk induced timing jitter of parallel microstrip lines,” IEEE Transactions on Advanced Packaging, vol. 31, 2008, pp. 809-817

[20] F. Gianesello, D. Gloria, C. Raynaud, S. Montusclat, S. Boret, C. Clement, C. Tinella, Ph. Benech, J.M. Fournier and G. Dambrine, “State of the art integrated millimeter wave passive components and circuits in advanced thin SOI CMOS technology on high resistivity substrate,” SOI Conference, 2005. Proceedings. IEEE International. IEEE, 2005. pp. 52-53

[21] Kim, Ki Hyeon, Shigehiro Ohnuma, and Masahiro Yamaguchi, “RF integrated noise suppressor using soft magnetic films,” IEEE transactions on magnetics 40.4, 2004, pp. 2838-2840

[22] Kijima, H., Ohnuma, S., Masumoto, H., Shimada, Y., Endo, Y., and Yamaguchi, M., “High noise suppression using magnetically isotropic (CoFe-AlN)/(AlN) multilayer

films," Journal of Applied Physics, 117, 17E514, 2015

[23] Chen, H. C., Lee, K. C., Lin, J. H., & Koch, M., "Comparison of electromagnetic shielding effectiveness properties of diverse conductive textiles via various measurement techniques," Journal of Materials Processing Technology 192, 2007, pp. 549-554

[24] Roh, J. S., Chi, Y. S., Kang, T. J., & Nam, S. W., "Electromagnetic shielding effectiveness of multifunctional metal composite fabrics," Textile Research Journal 78.9, 2008, pp. 825-835

[25] M. Crespo, N. Méndez, M. González, J. Baselga, J. Pozuelo, "Synergistic effect of magnetite nanoparticles and carbon nanofibres in electromagnetic absorbing composites," Carbon 74, 2014, pp. 63–72

[26] M. Han, X. Yin, H. Wu, Z. Hou, C. Song, X. Li, L. Zhang, and L. Cheng, "Ti_3C_2 MXenes with modified surface for high-performance electromagnetic absorption and shielding in the X-band," ACS applied materials & interfaces, 2016, 8.32, pp. 21011-21019

[27] B.-W. Li, Y. Shen, Z.-X. Yue, C.-W. Nan, "Enhanced microwave absorption in nickel/hexagonal-ferrite/polymer composites," Appl. Phys. Lett. 89, 132504, 2006

[28] Y. Li, R. Yi, A. Yan, L. Deng, K. Zhou, X. Liu, "Facile synthesis and properties of ZnFe2O4 and ZnFe2O4/polypyrrole core-shell nanoparticles," Solid State Sci. 11, 2009, pp. 1319–1324

[29] S. H. Hosseini, A. Asadnia, "Synthesis, characterization, and microwave-absorbing properties of polypyrrole/MnFe2O4 nanocomposite," J. Nanomater, 198973, 2012

[30] Zhang, H., Xie, A., Wang, C., Wang, H., Shen, Y., & Tian, X., "Novel rGO/α-Fe 2 O 3 composite hydrogel: synthesis, characterization and high performance of

electromagnetic wave absorption," Journal of Materials Chemistry A 1.30, 2013, pp. 8547-8552

[31] V. K. Sachdev, K. Patel, S. Bhattacharya, R. P. Tandon, "Electromagnetic interference shielding of graphite/acrylonitrile butadiene styrene composites," J. Appl. Polym. Sci. 120, 2011, pp. 1100–1105

[32] K. Batrakov, P. Kuzhir, S. Maksimenko, A. Paddubskaya, S. Voronovich, Ph Lambin, T. Kaplas & Yu Svirko, "Flexible transparent graphene/polymer multilayers for efficient electromagnetic field absorption," Scientific reports, 4, 2014, 7191

[33] Batrakov, K., Kuzhir, P., Maksimenko, S., Paddubskaya, A., Voronovich, S., Kaplas, T., & Svirko, Y., "Enhanced microwave shielding effectiveness of ultrathin pyrolytic carbon films," Applied Physics Letters, 103.7, 2013, pp. 073117

[34] W. Song, M. Cao, M. Lu, S. Bi, C. Wang, J. Liu, J. Yuan, L. Fan, "Flexible graphene/polymer composite films in sandwich structures for effective electromagnetic interference shielding," Carbon, 2014, 66: 67-76

[35] Shen, B., Zhai, W., Tao, M., Ling, J., & Zheng, W., "Lightweight, multifunctional polyetherimide/graphene@ Fe3O4 composite foams for shielding of electromagnetic pollution," ACS applied materials & interfaces, 2013, 5.21, pp. 11383-11391

[36] D. Yan, H. Pang, B. Li, R. Vajtai, L. Xu, P. Ren, J. Wang, Z. Li, "Structured Reduced Graphene Oxide/Polymer Composites for Ultra-Efficient Electromagnetic Interference Shielding," Advanced Functional Materials, 2015, 25.4, pp. 559-566

[37] A. Singh, P. Garg, F. Alam, K. Singh, R.B. Mathur, R.P. Tandon, Amita Chandra, S.K. Dhawan, "Phenolic resin-based composite sheets filled with mixtures of reduced graphene oxide, γ-Fe2O3 and carbon fibers for excellent electromagnetic interference shielding in the X-band," Carbon, 2012, 50.10, pp. 3868-3875

[38] B. Wen, M. Cao, M. Lu, W. Cao, H. Shi, J. Liu, X. Wang, H. Jin, X. Fang, W. Wang, J. Yuan, “Reduced graphene oxides: light-weight and high-efficiency electromagnetic interference shielding at elevated temperatures,” Advanced materials, 2014, 26.21,pp. 3484-3489

[39] Kumar, P., Shahzad, F., Yu, S., Hong, S. M., Kim, Y. H., & Koo, C. M., “Large-area reduced graphene oxide thin film with excellent thermal conductivity and electromagnetic interference shielding effectiveness,” Carbon, 2015, 94: 494-500

[40] Verma, M., Singh, A. P., Sambyal, P., Singh, B. P., Dhawan, S. K., & Choudhary, V., “Barium ferrite decorated reduced graphene oxide nanocomposite for effective electromagnetic interference shielding,” Physical Chemistry Chemical Physics, 2015, 17.3, pp. 1610-1618

[41] S. Hsiao, C. M. Ma, W. Liao, Y. Wang, S. Li, Y. Huang, R. Yang, and W. Liang “Lightweight and flexible reduced graphene oxide/water-borne polyurethane composites with high electrical conductivity and excellent electromagnetic interference shielding performance,” ACS applied materials & interfaces, 2014, 6.13, pp. 10667-10678

[42] Saini, P., Choudhary, V., Sood, K. N., & Dhawan, S. K., “Electromagnetic interference shielding behavior of polyaniline/graphite composites prepared by in situ emulsion pathway,” Journal of applied polymer science, 2009, 113.5, pp. 3146-3155

[43] AL-GHAMDI, Ahmad A.; EL-TANTAWY, Farid, “New electromagnetic wave shielding effectiveness at microwave frequency of polyvinyl chloride reinforced graphite/copper nanoparticles,” Composites Part A: Applied Science and Manufacturing, 2010, 41.11, pp. 1693-1701

[44] Yang, Y., Gupta, M. C., Dudley, K. L., & Lawrence, R. W., “Novel carbon nanotube−polystyrene foam composites for electromagnetic interference shielding,” Nano letters, 2005, 5.11, pp. 2131-2134

[45] N. Li, Y. Huang, F. Du, X. He, X. Lin, H. Gao, Y. Ma, F. Li, Y. Chen, and Peter C. Eklund, “Electromagnetic interference (EMI) shielding of single-walled carbon nanotube epoxy composites,” Nano letters, 2006, 6.6, pp. 1141-1145

[46] Y. Huang, N. Li, Y. Ma, F. Du, F. Li, X. He, X. Lin, H. Gao, Y. Chen “The influence of single-walled carbon nanotube structure on the electromagnetic interference shielding efficiency of its epoxy composites,” Carbon, 2007, 45.8, pp. 1614-1621

[47] H. M. Kim, K. Kim, C. Y. Lee, J. Joo, S. J. Cho, H. S. Yoon, D. A. Pejaković, J. W. Yoo, and A. J. Epstein, “Electrical conductivity and electromagnetic interference shielding of multiwalled carbon nanotube composites containing Fe catalyst,” Applied Physics Letters, 2004, 84.4, pp. 589-591

[48] GUPTA, Anju; CHOUDHARY, Veena, “Electromagnetic interference shielding behavior of poly (trimethylene terephthalate)/multi-walled carbon nanotube composites,” Composites Science and Technology, 2011, 71.13, pp. 1563-1568

[49] Cao, M. S., Song, W. L., Hou, Z. L., Wen, B., & Yuan, J., “The effects of temperature and frequency on the dielectric properties, electromagnetic interference shielding and microwave-absorption of short carbon fiber/silica composites,” Carbon, 2010, 48.3, pp. 788-796

[50] TZENG, Shinn-Shyong; CHANG, Fa-Yen, “EMI shielding effectiveness of metal-coated carbon fiber-reinforced ABS composites,” Materials Science and Engineering: A, 2001, 302.2, pp. 258-267

[51] AMELI, A.; JUNG, P. U.; PARK, C. B., “Electrical properties and electromagnetic

interference shielding effectiveness of polypropylene/carbon fiber composite foams," Carbon, 2013, 60, pp. 379-391

[52] Bayat, M., Yang, H., Ko, F. K., Michelson, D., & Mei, A., "Electromagnetic interference shielding effectiveness of hybrid multifunctional Fe_3O_4/carbon nanofiber composite," Polymer, 2014, 55.3, pp. 936-943

[53] Shimada, Y., Ma, J., Ito, T., Yanagi, K., Endo, Y., Muroga, S., & Yamaguchi, M., "Performance of crossed anisotropy multilayered CoZrNb films as IC chip level electromagnetic noise suppressor," IEEE Transactions on Magnetics, 2014, 50.11, pp. 1-4

[54] Kijima, H., Ohnuma, S., Masumoto, H., Shimada, Y., Endo, Y., & Yamaguchi, M., "High noise suppression using magnetically isotropic (CoFe-AlN)/(AlN) multilayer films," Journal of Applied Physics, 2015, 117.17, pp. 17E514

[55] Ono, H., Ito, T., Yoshida, S., Takase, Y., Hashimoto, O., & Shimada, Y., "Noble magnetic films for effective electromagnetic noise absorption in the gigahertz frequency range," IEEE transactions on magnetics 40.4 2004, pp. 2853-2857

[56] M. Naguib, M. Kurtoglu, V. Presser, J. Lu, J. Niu, M. Heon, L. Hultman, Y. Gogotsi, M. W. Barsoum, "Two-dimensional nanocrystals produced by exfoliation of Ti3AlC2. Advanced Materials," 2011, 23.37, pp. 4248-4253

[57] M Lukatskaya, O. Mashtalir, C. Ren, Y. Dall'Agnese, P. Rozier, P. L. Taberna, M. Naguib, P. Simon, M. W. Barsoum1, Y. Gogotsi, "Cation intercalation and high volumetric capacitance of two-dimensional titanium carbide," Science, 2013, 341.6153, pp. 1502-1505

[58] Ghidiu, M., Lukatskaya, M. R., Zhao, M. Q., Gogotsi, Y., & Barsoum, M. W., "Conductive two-dimensional titanium carbide 'clay'with high volumetric

capacitance," Nature, 2014, 516.7529: 78

[59] M. Yamaguchi, S. Tanaka, Y. Endo, S. Muroga and M. Nagata, "On-chip integrated magnetic thin-film solution to countermeasure digital noise on RF IC," Electromagnetic Compatibility (APEMC), 2015 Asia-Pacific Symposium on, IEEE, 2015, pp. 536-539

[60] M. Yamaguchi, Y. Endo, P. Fan, J. Ma, S. Tanaka, Y. Miyazawa and M. Nagata, "Analysis of patterned magnetic thin-film noise suppressor for RF IC chip," Electromagnetic Compatibility of Integrated Circuits (EMC Compo), 2017 11th International Workshop on IEEE, 2017, pp. 45-49

[61] M. Sho, Y. Masahiro, "RF joule losses analysis in thin film noise suppressor estimated by 3-D equivalent circuit network," IEEE Transactions on Magnetics, 2009, 45.10, pp. 4804-4807

[62] Muroga, S., Endo, Y., Mitsuzuka, Y., Shimada, Y., & Yamaguchi, M., "Estimation of peak frequency of loss in noise suppressor using demagnetizing factor," IEEE Transactions on Magnetics, 2011, 47.2, pp. 300-303

[63] F. Peng，Master's thesis，Tohoku University，2014

[64] T. Nakamura, S. Nagata, Anass Benjebbour, and Yoshihisa Kishiyama, "Trends in small cell enhancements in LTE advanced," IEEE Commun. Mag., vol. 51, no. 2, 2013, pp. 98-105

[65] Landy, N. I., Sajuyigbe, S., Mock, J. J., Smith, D. R., & Padilla, W. J., "Perfect metamaterial absorber. Physical review letters, 2008, 100.20: 207402

[66] Ding, F., Cui, Y., Ge, X., Jin, Y., & He, S., "Ultra-broadband microwave metamaterial absorber," Applied physics letters, 2012, 100.10: 103506

[67] Sabah, C., Dincer, F., Karaaslan, M., Unal, E., Akgol, O., & Demirel, E., "Perfect

metamaterial absorber with polarization and incident angle independencies based on ring and cross-wire resonators for shielding and a sensor application," Optics Communications, 2014, 322, pp. 137-142

[68] Zhang, Y., Duan, J., Zhang, B., Zhang, W., & Wang, W., "A flexible metamaterial absorber with four bands and two resonators," Journal of Alloys and Compounds, 2017, 705, pp. 262-268

[69] Karaaslan, M., Bağmancı, M., Ünal, E., Akgol, O., & Sabah, C., "Microwave energy harvesting based on metamaterial absorbers with multi-layered square split rings for wireless communications," Optics Communications, 2017, 392, pp. 31-38

[70] Lyu, J., Zhao, X., Hou, X., Zhang, Y., Li, T., & Yan, Y., "Electromagnetic interference shielding based on a high strength polyaniline-aramid nanocomposite," Composites Science and Technology 149, 2017, pp. 159-165

[71] Practical productions of graphene, supply and cost, https://www.springer.com/

[72] T. Ito, "CoZrNb 直交磁化膜の高周波特性(High frequency characteristics of crossed magnetic film CoZrNb)," The Institute of Electrical Engineers of Japan, 2013

[73] Auth C., Aliyarukunju A., Asoro M., Bergstrom D., Bhagwat V., Birdsall J., & Fu Q., "A 10nm high performance and low-power CMOS technology featuring 3 rd generation FinFET transistors, Self-Aligned Quad Patterning, contact over active gate and cobalt local interconnects," Electron Devices Meeting (IEDM), 2017 IEEE International. IEEE, 2017

Chapter 2
Evaluation system of magnetic film-type noise suppressor

2.1 Introduction

As mentioned in Ref. [59] of chapter 1, the magnetic film was deposited onto the passivation layer of an RF IC chip as a noise suppressor. A large number of metal lines such as signal, ground, power lines were constructed complexly. Previous studies have shown that inductive and conductive noise couplings mainly occurred between those lines. Therefore, in this chapter, we discuss a method to simplify the complicated chip into a common and simple model, which is basically a microstrip line covered by a magnetic film. A one-turn magnetic probe will be used to measure the magnetic field intensity in order to confirm the magnetic shielding effectiveness. A network analyzer will be used to measure the s-parameter in order to confirm the conductive loss (one line model) and crosstalk performance (two lines model). In addition, the noise suppression effect (including magnetic near-field shielding (one line model), conductive loss (one line model), and crosstalk (two lines model)) of magnetic films with different permeability

and resistivity will be measured by the proposed method.

2.2 Procedure

2.2.1 Measurement of inductive and conductive noise suppression

In order to study the mechanism of noise suppression of magnetic films, the complicated film-covered chip is simplified into two simple models as shown in Fig. 2.1. Firstly, for the study of near-field shielding and conductive loss, a microstrip line that is covered by a magnetic film is proposed as shown in Fig. (b). Second, in the aspect of crosstalk investigation, two paralleled microstrip lines that are covered by a magnetic film is proposed as shown in Fig. (c).

Figure 2.2 (a) shows a measurement method where a microstrip line is covered by a magnetic film in the middle. The two ports of the signal line are connected to a network analyzer (Keysight © E8362B) to measure the reflection and transmission coefficient. The frequency range is from 0.1 GHz to 10 GHz. Above the magnetic film, there is a magnetic probe (CP-2S) [1], which measures the magnetic field, intensity in the Y direction. The effective area of magnetic field induction is $1000 \times 200\ \mu m^2$. The magnetic probe is connected to two RF amplifiers (Keysight © 83006A and Keysight © 83051A) with gains 20 dB and 23 dB, respectively. The output of the amplifiers is connected to a spectrum analyzer (R&S ® FSU) which exports the magnetic field results by the unit of dBm.

As for the dimension of the microstrip line shown in Fig. 2.2 (b), the area of both ground (copper) and dielectric layer (SiO_2) are $10 \times 10\ mm^2$. The thickness of ground is 2 μm.

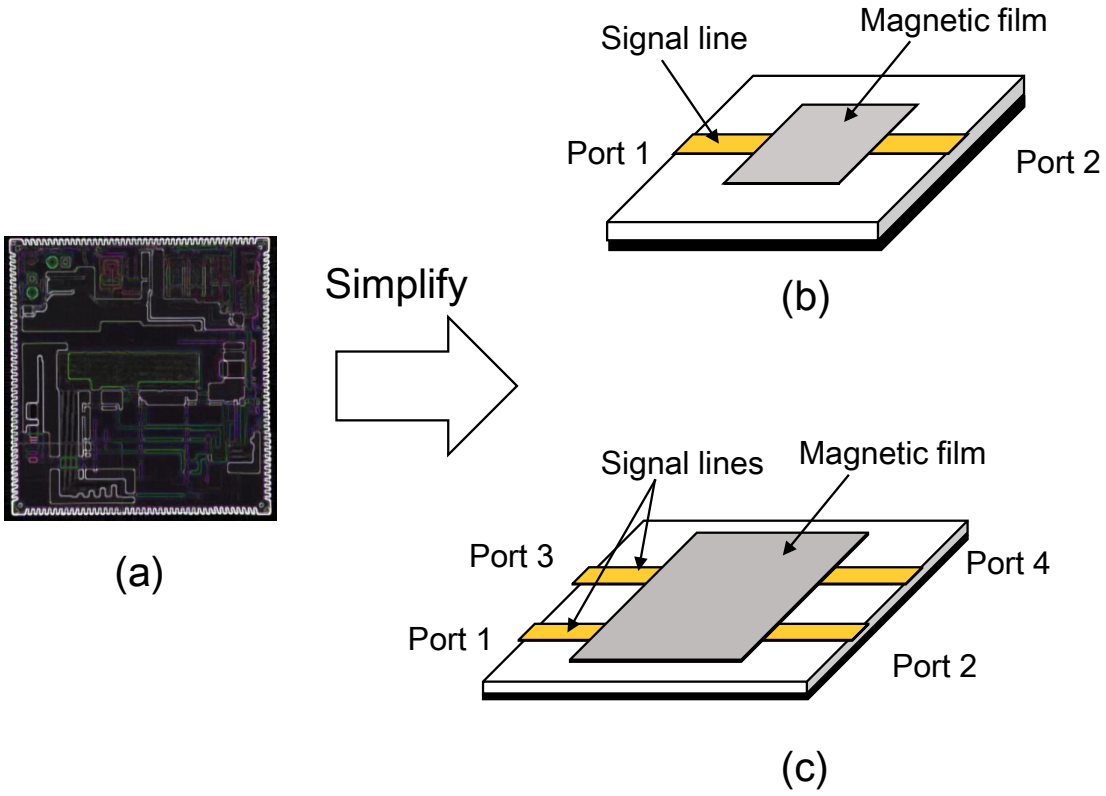

Fig. 2.1 The film-covered chip is simplified as (a) a microstrip line covered by a magnetic film, (b) two paralleled microstrip lines covered by a magnetic film

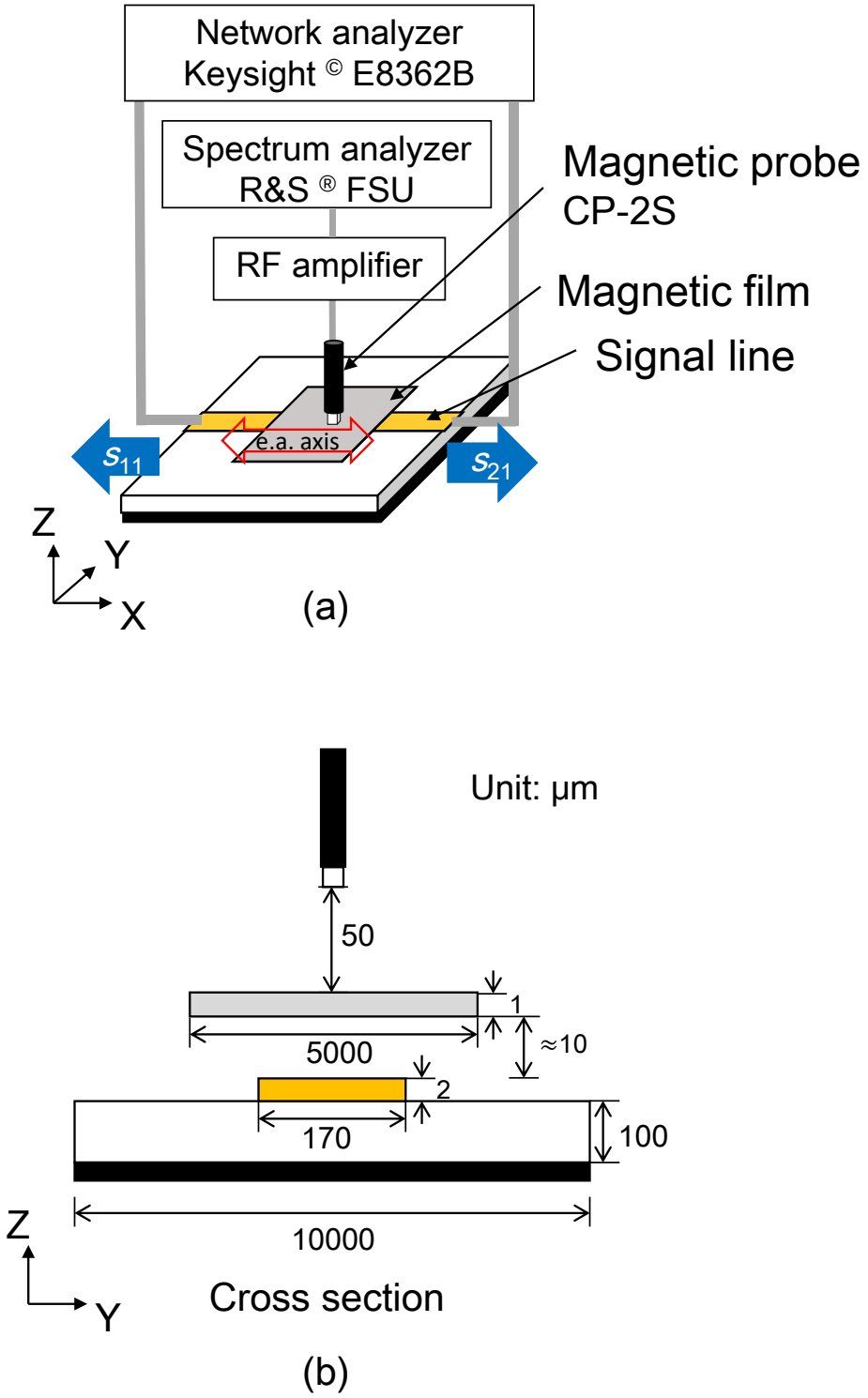

Fig. 2.2 Experimental setup 1, (a) a microstrip line that is covered by a magnetic film (b) cross section of the magnetic film-covered microstrip line.

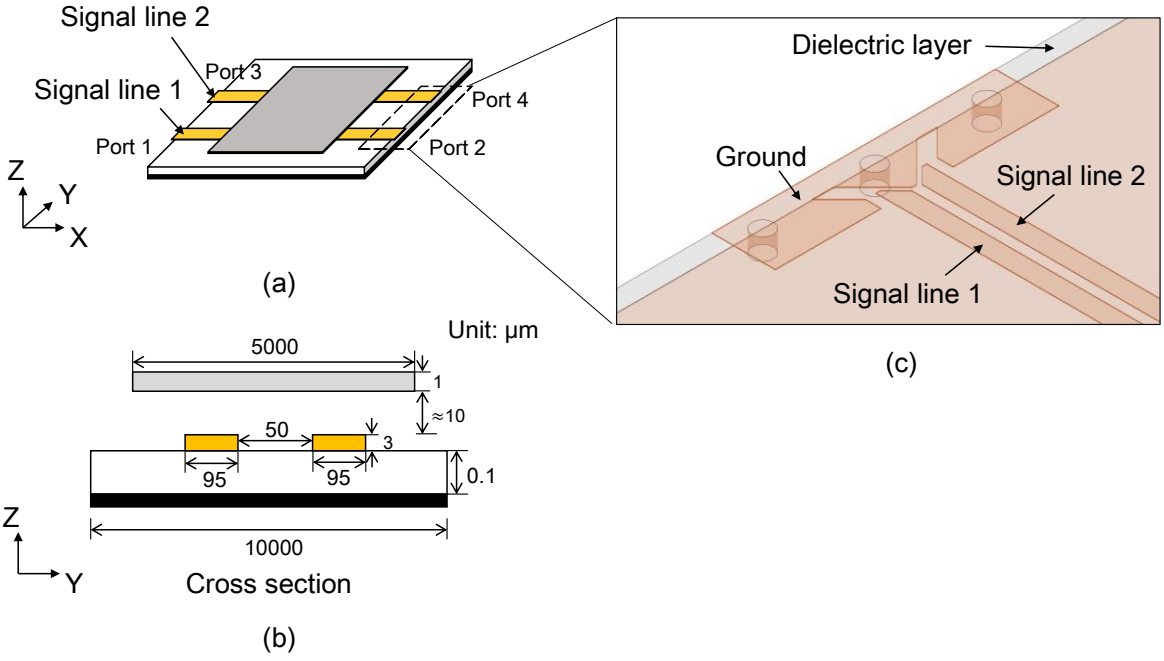

Fig. 2.3 Experimental setup 2, (a) design of two parallel microstrip lines, (b) cross section, (c) detailed structure of the signal port

The thickness of the dielectric layer is 100 μm. The width and thickness of the signal line is 170 μm and 2 μm. The magnetic film is placed about 10 μm above the signal line. The area of the magnetic film is $5 \times 5\ \mathrm{mm}^2$ while the thickness is around 1 μm. The magnetic probe is set about 50 μm high above the magnetic film in the center.

The shielding effectiveness (SE) is calculated by (2.1) which is the difference between the probe output without the magnetic film and that with the magnetic film. [2]

$$\mathrm{SE} = P_{\text{without film}} - P_{\text{with film}} \tag{2.1}$$

where $P_{\text{without film}}$ and $P_{\text{with film}}$ are the probe output (dBm) without a magnetic film and with a magnetic film, respectively. On the other hand, the conductive loss P_{loss}/P_{in} of magnetic film is calculated by (2.2),

$$P_{loss}/P_{in} = 1 - (|s_{11}|^2 + |s_{21}|^2) \tag{2.1}$$

where s_{11} is the reflection coefficient, s_{21} is the transmission coefficient. $P_{\text{loss}}/P_{\text{in}}$ is expected to have the same frequency spectrum as the shielding effect. Thus, both the shielding effect and conductive loss maybe analyzed simultaneously.

2.2.2 Measurement of crosstalk

The measurement setup of crosstalk performance is designed as shown in Fig. 2.3. Two paralleled signal lines are designed having the same size and the gap between them is 50 μm. The width and thickness of each signal line is 95 μm and 3 μm. The area of the ground and dielectric layer is same as the one line design mentioned in chapter 2.1.1. On one side of the ports as shown in Fig. 2.3 (c), three holes were made to connect

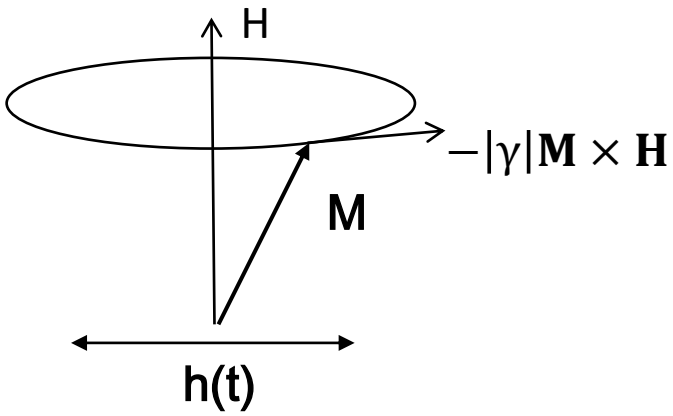

α: Gilbert dumping

γ: Gyromagnetic ratio

Fig. 2.4 Magnetic moment moves as processing when $h(t)$ is applied

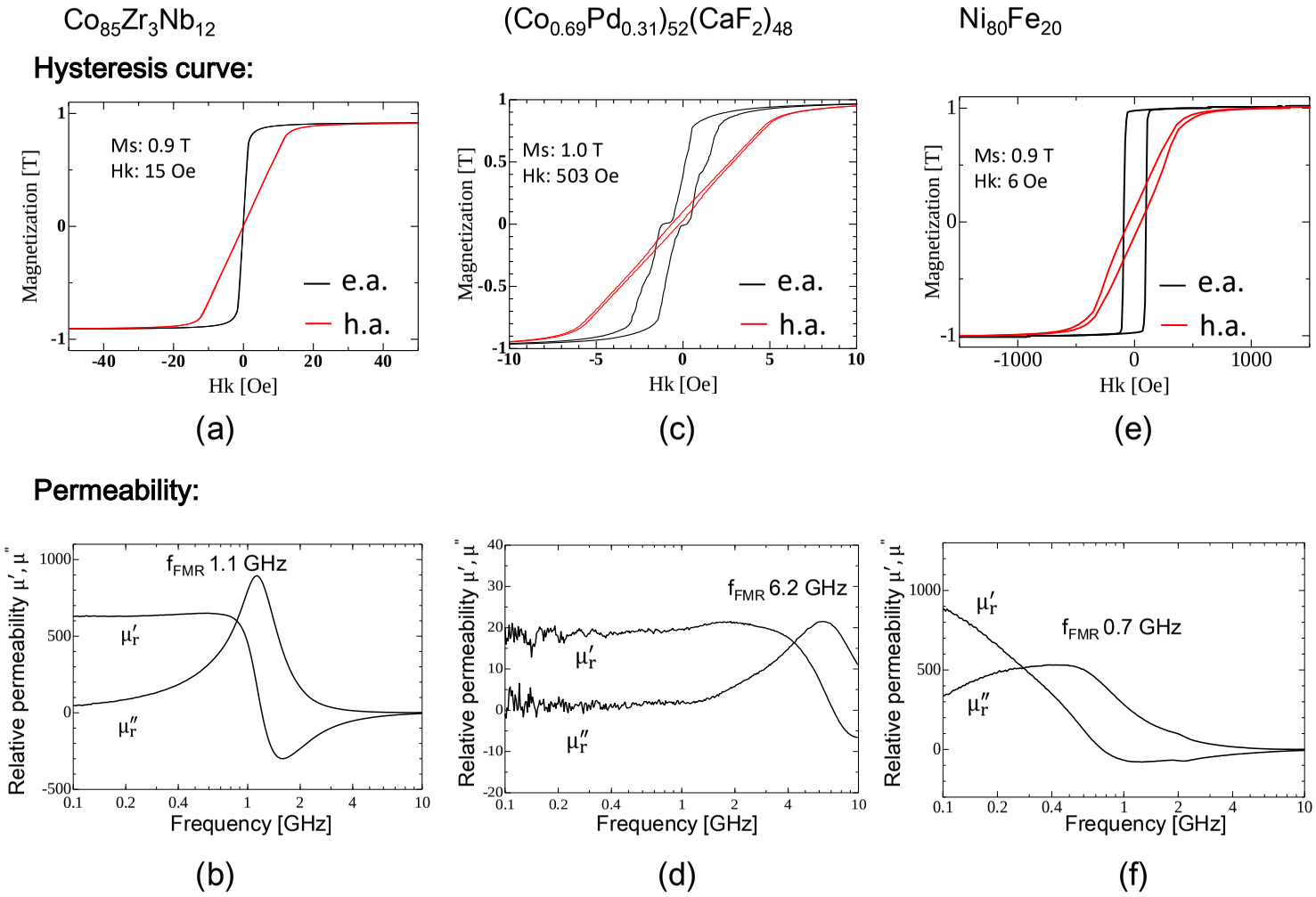

Fig. 2.5 M-H curves and permeability. (a) (c) (e) Hysteresis curve of Co-Zr-Nb film, Co-Pd film, and Ni-Fe film, (b) (d) (f) frequency dependence of permeability of Co-Zr-Nb film, Co-Pd film, and Ni-Fe film.

the bottom surface ground to the upper surface ground, so as to lay the ground part on the same plane as the signal line. Thus, wafer probes are used to connect the ports and network analyzer. Magnetic films of the same size are also placed about 10 μm above the signal lines.

One of the lines is acts as an aggressor which has an input and output signal provided by the network analyzer. The other line acts like a victim, which does not have any input signal. The frequency range is the same as before i.e., from 0.1 GHz to 10 GHz.

Based on this design, the near-end crosstalk s_{31} and far-end crosstalk s_{41} will be measured.

2.3 Magnetic films

2.3.1 Processing of magnetic moments

The easy axis is put parallel to the signal line (the transmission direction); this ensures the applied magnetic field $h(t)$ is vertical to the direction of magnetization *H*. Through this, the processing will occur in magnetic moments *M* and thus the FMR of the magnetic film can work properly as shown in Fig. 2.4 [4].

There are three types of magnetic films used in this study. Each of them has a different relative permeability and resistivity. All three films have the same area and thickness, i.e., 5×5 mm^2 and 1 μm , respectively. The details will be introduced in the next three parts.

2.3.2 Co-Zr-Nb magnetic film

The $Co_{85}Zr_3Nb_{12}$ amorphous film was fabricated via sputtering and deposited on a SiO_2 substrate. The film structure was composed of a stack of SiO_2 layers (100 nm) / [Co-

Zr-Nb (250 nm) / SiO_2 (10 nm)] ×4. The hysteresis curve is shown in Fig. 2.5 (a), where the magnetic anisotropy field H_k is about 1.2 kOe and the saturation magnetization $4\pi M_s$ is 0.9 T. The resistivity ρ is 1.2×10^{-6} Ω·m. Furthermore, the frequency dependence of permeability μ of Co-Zr-Nb film is shown in Fig. 2.5 (b). It has a constant real part μ_r', which is about 630 at low frequency, and exhibits the maximum imaginary part μ_r'', which is about 890 at the FMR frequency of 1.1 GHz.

2.3.3 CoPd-CaF_2 Nanogranular magnetic film

Another magnetic film used in this study is $(Co_{0.69}Pd_{0.31})_{52}$-$(CaF_2)_{48}$ film (hereafter Co-Pd film) [1]. It is constructed by magnetic metal partials that are surrounded by the insulator ceramic matrix. The film is single layered and its thickness is about 1 μm. The hysteresis curve is shown in Fig. 2.5 (c), where the magnetic anisotropy field H_k is about 40 kOe and the saturation magnetization $4\pi M_s$ is about 1 T. The resistivity ρ is 2.9×10^{-6} Ω·m. The frequency dependence of permeability for the Co-Pd film is shown in Fig. 2.5 (d). The FMR frequency is located at about 6.2 GHz when the imaginary part of permeability is maximum i.e., 22. The real part of permeability is around 20.

2.3.4 Ni-Fe magnetic film

The third one is the Permalloy film that is composed of $Ni_{80}Fe_{20}$. It has the same structure as that of Co-Zr-Nb film, which is also a stack of SiO_2 layers (100 nm) / [Ni-Fe (250 nm) / SiO_2 (10 nm)] ×4. The hysteresis curve is shown in Fig. 2.5 (e), where the magnetic anisotropy field H_k is about 0.48 kOe and the saturation magnetization $4\pi M_s$ is about 0.9 T. The resistivity ρ is 0.2×10^{-6} Ω·m. The frequency dependence of permeability for the Ni-Fe film is shown in Fig. 2.5 (f). The FMR frequency is located at

around 0.7 GHz when the imaginary part of permeability is the maximum, around 500. At low frequency, the real part of permeability is around 1000. Then, in the frequencies above 0.1 GHz, it smoothly decreases, which is in contrast to the sharp reduction in the case of Co-Zr-Nb film. This is considered to be the consequence of decentralized magnetic moment inside the Ni-Fe film.

2.3.5 Permeability and resistivity difference

Comparing the three types of magnetic films, first, in the low frequency where the imaginary part of μ is nearly 0, Ni-Fe film has the highest real part of μ while Co-Pd film has the lowest. Further, the Co-Pd film has the highest resistivity that is 2.9×10^{-6} Ω·m, the second highest is that of the Co-Zr-Nb film and the lowest one belongs to the Ni-Fe film. Finally, because of the largest anisotropy field, the Co-Pd film has the highest FMR frequency, which is located at 6.2 GHz. The second highest FMR frequency belongs to the Co-Zr-Nb film and the lowest one is belong to the Ni-Fe film. The inductive/conductive noise suppression and crosstalk performance of three types of magnetic films are considered different because of their different permeability and resistivity.

2.4 Inductive and conductive noise suppression of complex permeability

2.4.1 Inductive noise suppression

In general, magnetic flux is concentrated in objects with high magnetic permeability.

Fig. 2.6 (a) shows the concept distribution of magnetic flux without the film and with the film. Owing to the high permeability that the magnetic film has, the magnetic flux is mainly concentrated in the film area and thus has a shielding effect on the outside space. Fig. 2.6 (b) shows the absolute value of complex permeability along with the frequency of magnetic films, where the maximum value of absolute permeability is at the FMR frequency. Therefore, the magnetic flux is mostly concentrated inside the magnetic film when the signal frequency is equal to the FMR frequency, thus the maximum shielding effect is expected to occur at FMR frequency. [3]

2.4.2 Conductive noise suppression

The imaginary part of impedance X of the whole model when the microstrip line is covered by a magnetic film is calculated as,

$$j\omega L = j\omega\left(\frac{\mu_0\mu' S}{l} - j\frac{\mu_0\mu'' S}{l}\right) = \omega\frac{\mu_0\mu'' S}{l} + j\omega\frac{\mu_0\mu' S}{l} = R_m + j\omega L_m \tag{2.2}$$

where ω is the angular frequency, L is the inductance, μ_0 is the permeability of vacuum, S is the area of the magnetic circuit, and l is the length of the magnetic circuit. $R_m = \omega\frac{\mu_0\mu'' S}{l}$ is the resistance brought about by the imaginary part of permeability and is proportional to the imaginary part of permeability μ''. As shown in Fig. 2.7, the resistance of the whole line that is covered by the magnetic film increases by increasing the μ''. Because the maximum value of μ'' is located at the FMR frequency, the maximum resistance is generated at the same FMR frequency and thus leads to maximum power consumption of the magnetic film. The magnetic film acts like a band pass filter, which can convert the electrical power into heat and dissipate it [3].

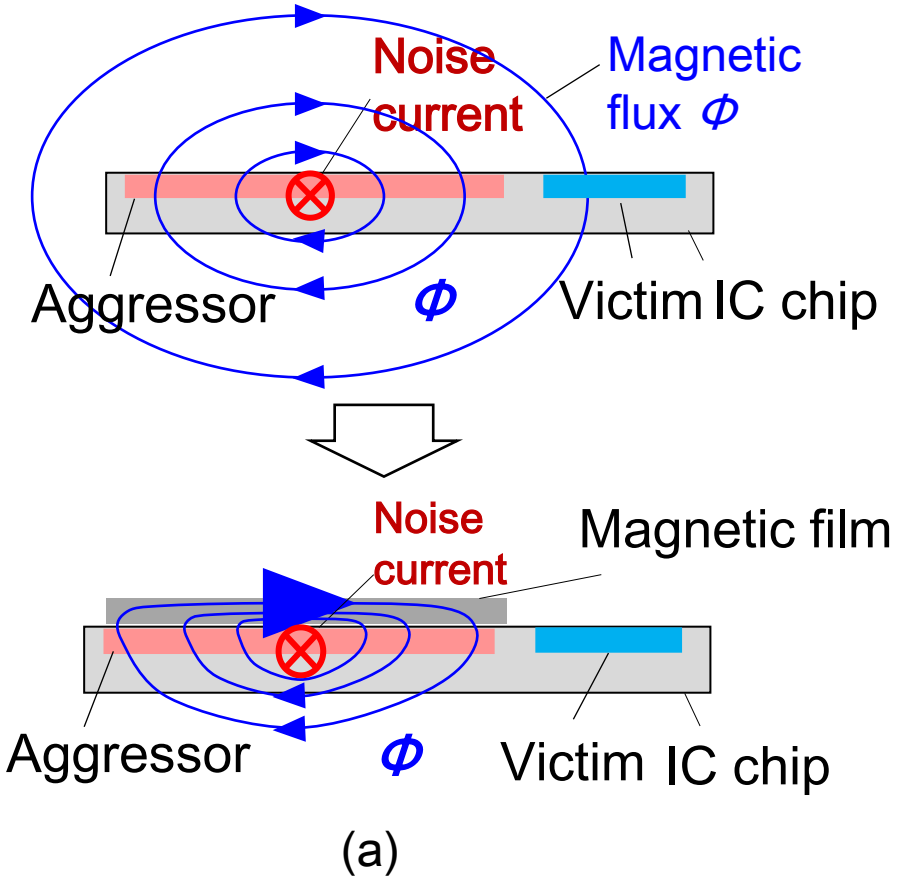

(a)

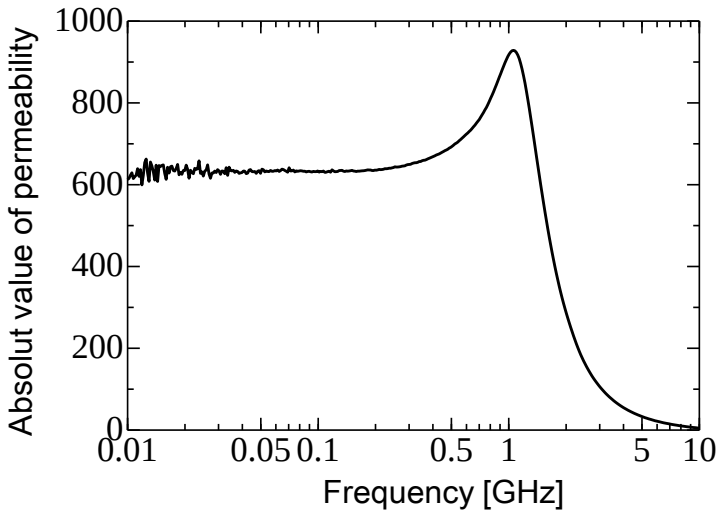

(b)

Fig. 2.6 (a) Distribution of magnetic flux without the magnetic film and that with the magnetic film, (b) absolute value of permeability of the magnetic film

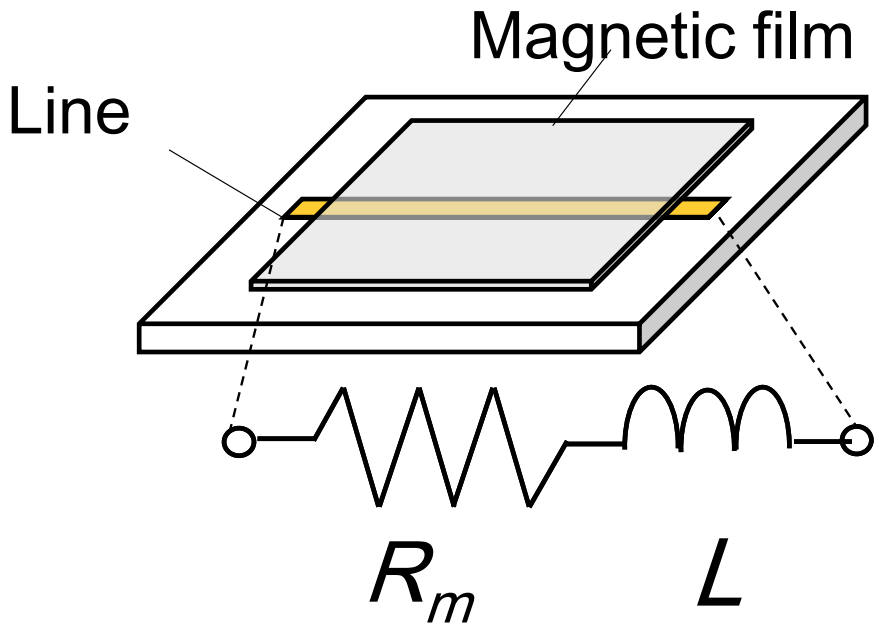

Fig. 2.7 resistance and inductance of the whole signal line that is covered by magnetic film

2.5 Experimental results of shielding effect and conductive loss

2.5.1 Measured results of shielding effect

Based on the proposed method mentioned in chapter 2.1, the measured shielding effectiveness is shown in Fig. 2.8 (a), where X-axis is the signal frequency and Y-axis is the magnetic shielding effectiveness.

In Fig. 2.8 (a), the red dotted line is the result of Co-Zr-Nb film. The shielding effect increases along with frequency and has a peak value of 14 dB at the frequency around 1.1 GHz of the intrinsic FMR frequency. Then, the shielding effect decreases along with frequency and has the lowest value of 2 dB at around 2 GHz. Finally, above 2 GHz, the shielding effect increases with frequency. The maximum shielding effect at around 1.1 GHz corresponds to FMR frequency of Co-Zr-Nb film.

The green dotted line is the result of the Co-Pd film. The shielding effect increases along with the frequency from 0.1 GHz to 10 GHz. Owing to the low value of permeability of the Co-Pd film, it cannot provide peak shielding like the Co-Zr-Nb film, as shown in Fig. 2.5.

The blue dotted line is the result of the Ni-Fe film, which linearly increases along with frequency and has a little dip at around 2.1 GHz. This dip is similar to that of the Co-Zr-Nb film. Since there is no maximum peak shielding effect observed, the decentralized magnetic moment of the Ni-Fe film is considered to be the reason. The decentralized magnetic moment also leads to the permeability shown in Fig. 2.5.

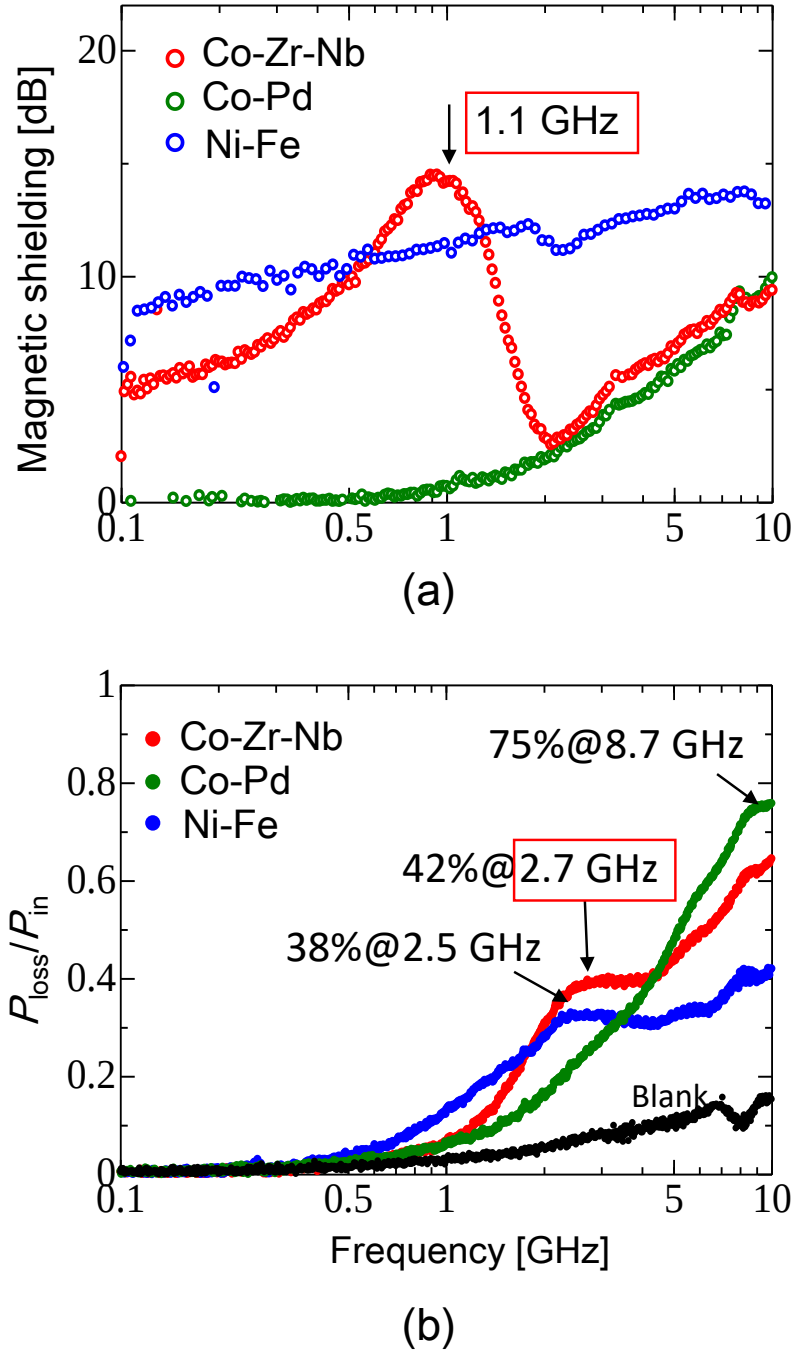

Fig. 2.8 (a) Measurement results of magnetic shielding effect, (b) frequency dependence of permeability, (c) conductive loss Ploss/Pin, of Co-Zr-Nb film, Co-Pd film, and Ni-Fe film.

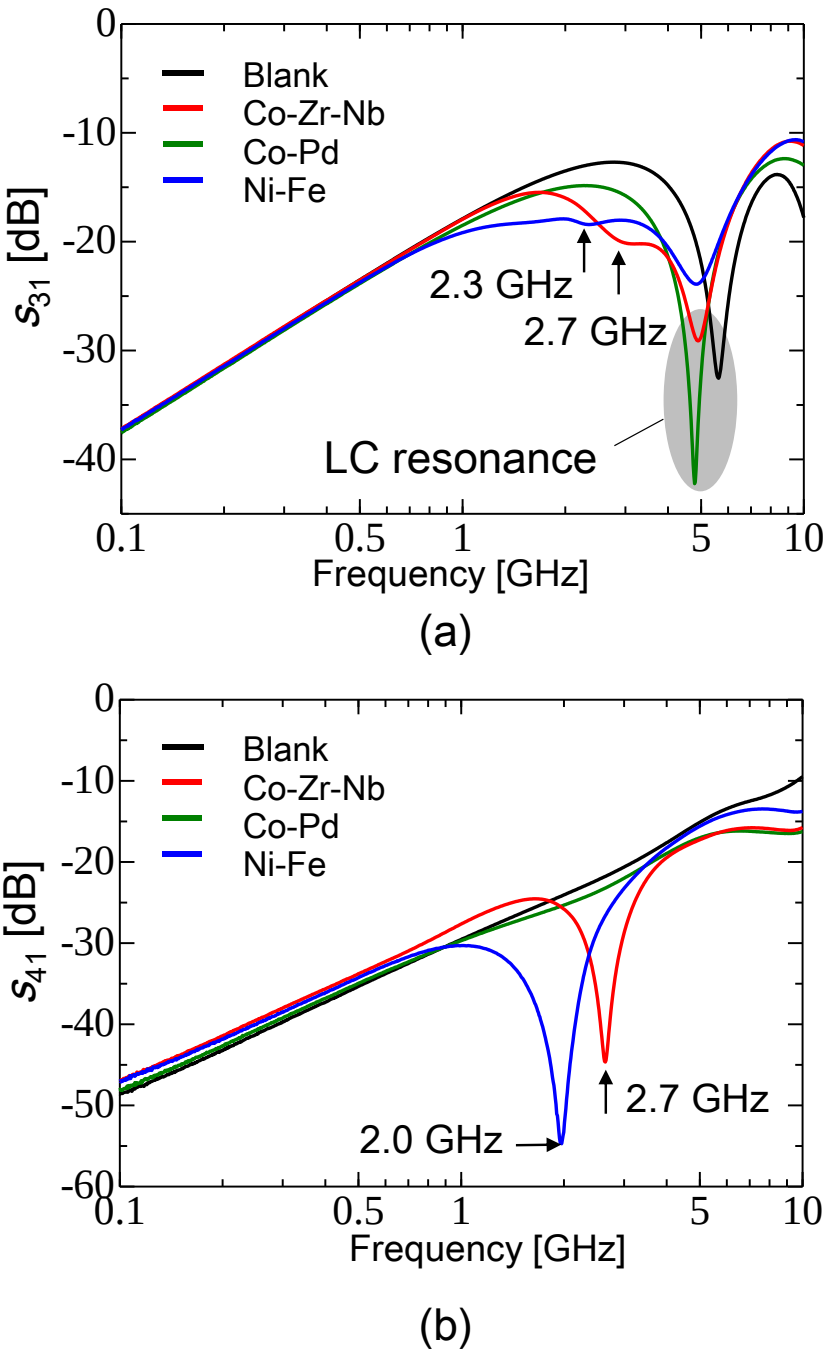

Fig. 2.9 Measured results of (a) near-end crosstalk, (b) far-end crosstalk

2.5.2 Measured results of conductive loss P_{loss}/P_{in}

Figure 2.8 (b) shows the measurement results of conductive loss $P_{loss}/P_{in,}$ which represents the percentage of power consumption of the magnetic film.

In the result of the Co-Zr-Nb film, shown as red solid line, P_{loss}/P_{in} increases along with frequency and has a maximum value of 42 % at around 2.7 GHz. A similar result is further obtained when the magnetic film used is either Ni-Fe film or Co-Pd film, which are shown as blue and green solid lines, respectively. Each of them has a maximum value of 38 % and 75 % at about 2.5 GHz and 8.7 GHz, respectively. The black solid line is the result of blank, the value of which is lower than any of the film-covered results.

A comparison of the shielding effect and conductive loss of the Co-Zr-Nb film reveals that the frequency of maximum shielding is different from that of the maximum conductive loss P_{loss}/P_{in}. The study about the mechanism of shielding effect and conductive loss will be discussed in chapter 3.

2.5.3 Crosstalk performance

In reference to the crosstalk method described in chapter 2.1.2, the measured results of near-end crosstalk s_{31} and far-end crosstalk s_{41} are shown in Fig. 2.9 (a) (b). The black lines are the results of blank. The red, green, and blue lines are the results of Co-Zr-Nb film, Co-Pd film, and Ni-Fe film, respectively.

In all the results of near-end crosstalk s_{31}, dips exist in the frequency range of 4.5 GHz to 6 GHz. These dips are considered to be the consequence of LC resonance. The dip-frequencies owing to the films are slightly shifted when compared to that of blank, which is considered to be the result of additional inductance and capacitance brought about by the magnetic film. Furthermore, in the result of Co-Zr-Nb film, another dip exists at

around 2.7 GHz. Similarly, in the results of Ni-Fe film, near-end crosstalk s_{31} is nearly flat from 1 GHz to 4 GHz, and there is a small dip at around 2.3 GHz.

On the other hand, in all the results of far-end crosstalk s_{41}, the lines of blank and Co-Pd film approximately increase along with the frequency, while there are dips at around 2.0 GHz and 2.7 GHz in each of the results of the Co-Zr-Nb film and Ni-Fe film. Because the value of the Co-Pd film is very small compared to the Co-Zr-Nb film and Ni-Fe film, the effect of permeability of the Co-Pd film is small. Thus, the result of the Co-Pd film is similar to that of blank and no dip exists. From the results, the influence of permeability is believed to be the reason of dips that arrowed in Fig. 2.9 (a) (b). The detail mechanism analysis will be discussed in chapter 4.

2.6 Summary

In this chapter, a method that can systematically evaluate both the near-field shielding and conductive loss of a magnetic film simultaneously was proposed. The results of shielding effect and conductive loss are as expected from the general mechanism explanation. Hence, the validity of the proposed experiment is confirmed.

The new method can help evaluate the relationship of inductive and conductive noise suppression, which is an advantage over the previous studies. The inductive noise suppression, conductive noise suppression, and crosstalk of magnetic films with different permeability and resistivity were confirmed.

With respect to near-field shielding, Co-Zr-Nb film has a peak shielding value of 14 dB at the frequency around 1.1 GHz, which corresponds to FMR frequency of the Co-Zr-Nb film. The Co-Pd film shows exponential growth in the shielding effect along the whole

frequency range from 0.1 GHz to 10 GHz, which is owing to the low value of permeability. The Ni-Fe film has a nearly linear growth shielding effect along with frequency, which is considered to be the result of the decentralized magnetic moment of the Ni-Fe film.

Second, in the aspect of conductive loss, Co-Zr-Nb film has a maximum P_{loss}/P_{in} at about 2.7 GHz while similar peaks are obtained when the magnetic films are either Ni-Fe film or Co-Pd film. Each of them has a maximum value 38 % and 75 % at around 2.5 GHz and 8.7 GHz, respectively.

Finally, in the aspect of near-end crosstalk s_{31} and far-end crosstalk s_{41}, magnetic film with high permeability shows good suppression at particular frequencies. Except for the results of LC resonance, the Co-Zr-Nb film has two suppression dips at around 2.7 GHz in both s_{31} and s_{41}. The Ni-Fe film has a small dip at around 2.3 GHz in s_{31} and a large dip at 2 GHz in s_{41}. Those suppressions are considered the result of high permeability that magnetic film possesses.

References

[1] Naoe, M., Kobayashi, N., Ohnuma, S., Iwasa, T., Arai, K. I., Masumoto, H., “Ultra-high resistive and anisotropic CoPd–CaF2 nanogranular soft magnetic films prepared by tandem-sputtering deposition,” Journal of Magnetism and Magnetic Materials, 2015, 391, pp. 213-222

[2] Ono, H., Ito, T., Yoshida, S., Takase, Y., Hashimoto, O., & Shimada, Y., “Noble magnetic films for effective electromagnetic noise absorption in the gigahertz frequency range,” IEEE transactions on magnetics, 2004, 40.4, pp. 2853-2857

[3] Yamaguchi, M., Endo, Y., Tanaka, S., Ito, T., Muroga, S., Azuma, N., & Nagata, M., “On-chip magnetic thin-film noise suppressor for IC chip level digital noise countermeasure,” Electromagnetic Compatibility, Tokyo (EMC'14/Tokyo), 2014 International Symposium on. IEEE, 2014. pp. 354-357

[4] K. Ohta, “磁気工学の基礎Ⅰ，Ⅱ(Basics of magnetics engineering Ⅰ，Ⅱ),” Kyoritsu Shuppan Co., Ltd., 1973

Chapter 3
Mechanism analysis of inductive and conductive noise suppression

3.1 Introduction

In order to develop a finer magnetic film as a better noise suppressor that used in IC chip, the mechanism study of noise suppression effect of magnetic film is significant. In previous study, equivalent circuits were established based on the model that a coplanar waveguide covered by a magnetic film [1] [2]. The FMR property and eddy/displacement current (joule loss) were studied separately to explain the inductive and conductive noise suppression effect of magnetic film. The maximum shielding effect was explained the result of magnetic circuit resonance. However, the quantitative interactive between material property and noise suppression effect needs to be clarified.

From Shimada et al. [3], a microstrip line (hereafter MSL) with an eight-layer crossed-anisotropy Co-Zr-Nb film on the top is chosen as a basic structure to substitute the complicated film-integrated RF IC chip which is consisted of many power and ground lines. The in-plane noise suppression due to FMR phenomenon was found taking a major

role over a wide frequency range as demonstrated in [3]. However only the qualitative agreement was obtained between experimental and numerical simulation results. The quantitative relationship between near field suppression and FMR is needed to be verified.

Hence, this chapter is aimed to clarify the mechanism of shielding effect and conductive loss quantitatively from the aspect of material characteristic. Based on the experimental results of three kinds of magnetic film mentioned in chapter 2, Co-Zr-Nb film has a maximum shielding effect at 1.1 GHz, a maximum conductive loss at around 2.7 GHz, and crosstalk suppression dip at around 2.7 GHz. These good noise suppression capabilities are the most obvious results than that of two others. Thus, Co-Zr-Nb film is choose as a presentative in the mechanism study in this chapter.

Extensively, the mechanism of near field shielding will be discussed by means of loss distribution between eddy current and frequency-dependent complex permeability in simulation along with the frequency range of 0.1 to 10 GHz. In addition, based on the control of resistivity and the permeability in the simulation, the contribution of each mechanism to noise suppression effect will be clarified.

3.2 Simulation setup

3.2.1 Model establishment

A full wave electromagnetic simulation model as shown in Fig. 3.1 (a) has been established that has a same structure and dimension with the experiment. Fig. 3.1 (b) shows the details, where SMA ports are substitute by wave port setting to provide the signal input and output. The magnetic probe is replaced by a plane which has the same area with the effective area of magnetic probe. By calculating the average value of

magnetic field that pass through the plane, the simulated probe output could be exported. The magnetic flux through the plane can be calculated as

$$\phi = \int B(t)dS = \int \mu_0 H(t)dS = \mu_0 SH(t) \tag{3.1}$$

where ϕ is magnetic flux, $B(t)$ is magnetic flux density, μ_0 is vacuum permeability, and S is the area of plane which is the same size with experimental sensing coil (1000×200 μm^2) , $H(t)$ is magnetic field intensity. Then, the voltage of the plane is calculated as

$$V = \frac{d\phi}{dt} = \mu_0 S \frac{dH(t)}{dt} = \mu_0 S\omega H_{av} \tag{3.2}$$

where $\omega = 2\pi f$ is the angular frequency, H_{av} is the average magnetic field intensity through the plane. Finally, the power of probe output is showed as

$$P = \frac{(AV)^2}{R} \tag{3.3}$$

where A is the amplification factor, R is the characteristics resistance of which the value is 50 Ω.

In the process of meshing, because of the big difference between the size of thickness (z axis) and that of area (plane of xy axis), it's hard to mesh the model automatically and simultaneously keep the calculation accuracy. Therefore, this study builds rectangles on xy directions to cut the model and thus the number of mesh will be increased. As the results, the number of rectangles is 40 in x direction and 40 in y direction. The space between each rectangles is 0.5 mm as shown in Fig. 3.2. The total number of mesh

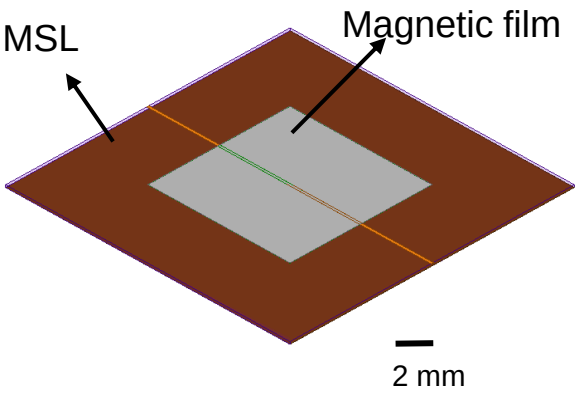

(a)

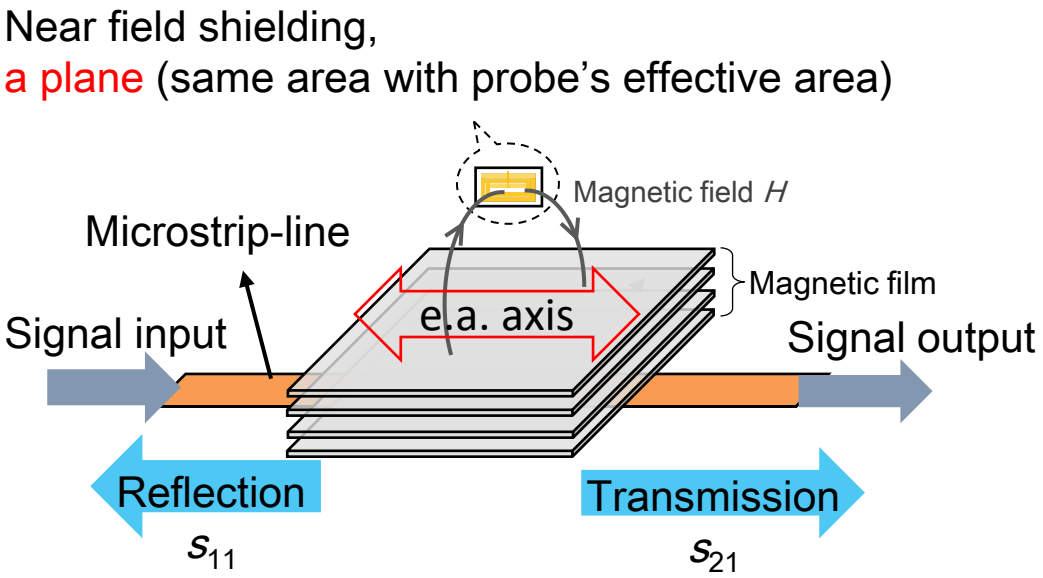

(b)

Fig. 3.1 Full wave electromagnetic simulation model. (a) The same dimension and structure with the experiment. (b) A plane that has the same area with probe's effective area

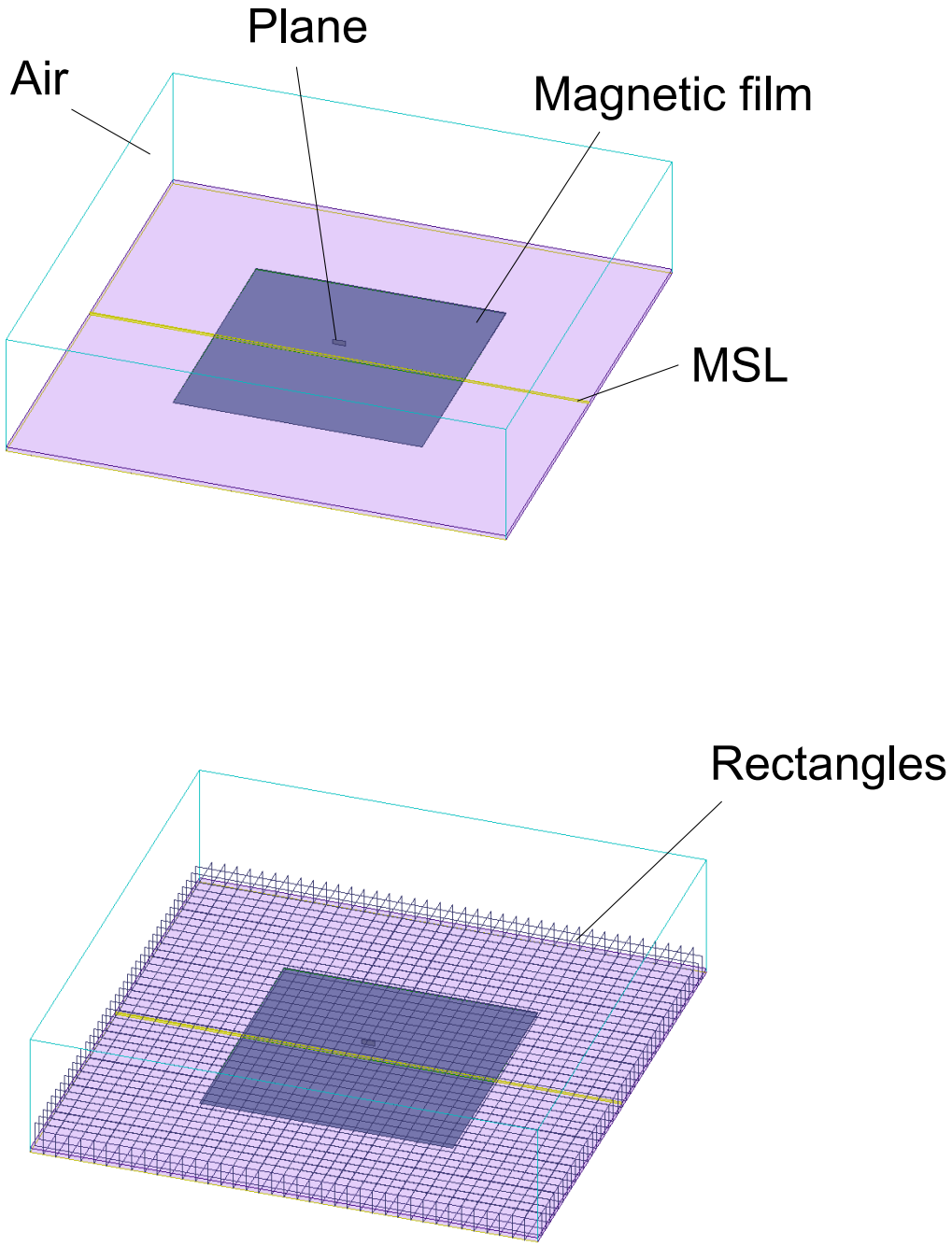

Fig. 3.2 Rectangles (40 x 40) are created in the simulation to cut the model and thus increase the number of mesh

elements is about 1.0 million while the average analysis time is about 20 hours.

On the other hand, in the simulation, the permeability of magnetic film is imported by the calculation results of Landau–Lifshitz–Gilbert (LLG) equation [4]

$$\frac{dM}{dt} = -\gamma[M \times H] - \frac{\alpha\gamma}{M}[M \times [M \times H]] \tag{3.4}$$

where M is magnetic moment, H is magnetic field, γ is gyromagnetic ratio, and α is dumping coefficient. The solution of (3.4) is shown as

$$\mu_{dc}{}' = \frac{\gamma M\omega_0(\omega_0^2-\omega^2)+\gamma M\omega^2\alpha^2\omega_0}{[\omega_0^2-\omega^2(1+\alpha^2)]^2+4\omega_0^2\omega^2\alpha^2} \tag{3.5a}$$

$$\mu_{dc}{}'' = \frac{\gamma M\omega\alpha[\omega_0^2+\omega^2(1+\alpha^2)]}{[\omega_0^2-\omega^2(1+\alpha^2)]^2+4\omega_0^2\omega^2\alpha^2} \tag{3.5b}$$

where $\mu_{dc}{}'$ is the real part of permeability, $\mu_{dc}{}''$ is the imaginary part of permeability, ω is angular frequency of applied magnetic field.

Additionally, the eddy current loss is considered significant in the permeability's calculation which will lead to the dispersion of μ. Thus based on [5], the permeability is calculated as

$$\mu_f = \mu_{dc}\, tanh\left(\frac{Pd}{2}\right) / \frac{Pd}{2} \tag{3.6}$$

where μ_f is the permeability under the consideration of eddy current, d is the thickness of magnetic film, and P is calculated as

$$P = (\frac{j\omega\mu_{dc}}{\rho})^{1/2} \tag{3.7}$$

Based on (3.5)-(3.7), the permeability of magnetic film is calculated as shown in the broken lines in Fig. 3.3. It is similar to the measured permeability. By importing the calculated permeability in the x direction of magnetic film, the easy axis is set to be x direction. Hence the magnetic film will work properly based on the calculation of Maxwell's equation.

3.2.2 Mechanism discussion and assumed cases

Three kinds of parameters are mainly considered contributing to the noise suppression effect of magnetic film. They are (1) classic magnetic shielding (2) eddy current loss and (3) FMR loss.

(1) Classical magnetic shielding

The conventional magnetic shielding is mainly depended on the high relative permeability ($\mu_r > \mu_0$) the magnetic material has. The magnetic flux will be concentrated inside the magnetic material because of the low reluctance path for the flux [6].

(2) Eddy current loss

When an AC magnetic field is applied to magnetic film, the electromotive force e is generated as

$$e = -\frac{\partial B}{\partial t} \tag{3.8}$$

where *B* is time dependent magnetic flux density. Thus, current is generated in the film

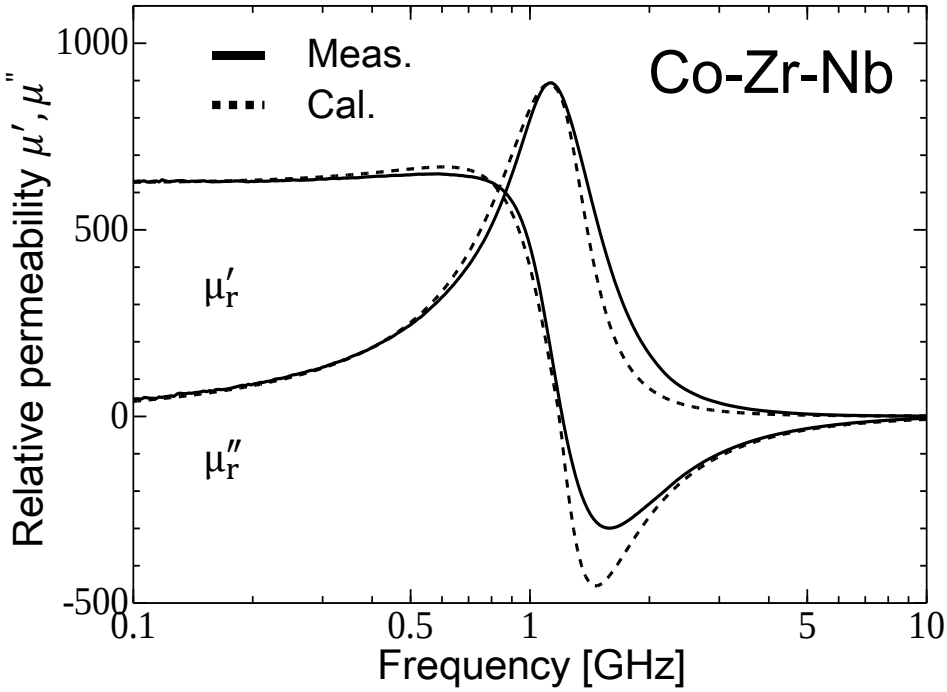

Fig. 3.3 Calculated permeability that similar to the measurement was imported to simulation, in order to unsure the proper working of magnetic film

which is called eddy current. The electrical energy is changed to Joule heat and dissipated in the film.

The eddy current will increase when the frequency of ambient magnetic field increases, and when the resistivity of film decreases. In this study, the magnetic film is divided from 1 layer (with thickness 1 μm) to 4 layers (with thickness of each 250 nm) in order to decline the eddy current. The SiO_2 is inserted into each layer as insulators with thickness of 10 nm. On the other hand, the multilayered structure is also aimed to prevent the asynchronous of magnetic moment, which can maintain smooth curves (without any undulation) of permeability [7].

(3) FMR loss

FMR loss is represented by the imaginary part $\mu_r''(f)$ of permeability. The equivalent circuit of the model in this study (microstrip line covered with magnetic film) is shown as Fig. 2.5. The magnetic resistance R is

$$R = \frac{l}{\mu_0 \mu_r S} \tag{3.9}$$

where l is the distance of magnetic flux path, μ is the permeability, S is the area of cross section. Then, the permeability of magnetic film is frequency dependent $\mu_r(f) = \mu_r'(f) - j\mu_r''(f)$, where $\mu_r'(f)$ is the real part and $\mu_r''(f)$ is the imaginary part. Thus, the inductance $L(f)$ of magnetic circuit is shown as

$$L(f) = \frac{N^2}{R} = \frac{\mu_0 \mu_r S N^2}{l} = \frac{\mu_0 \mu_r'(f) S N^2}{l} - j\frac{\mu_0 \mu_r''(f)\, S N^2}{l} \tag{3.10}$$

where N is the number of turns. Then, the impedance X is shown as equation (2.2) as the same description in chapter 2.4.2.

Based on the experimental results of three kinds of magnetic film mentioned in chapter 2, Co-Zr-Nb film has a maximum shielding effect at 1.1 GHz, a maximum conductive loss at around 2.7 GHz, and crosstalk suppression dip at around 2.7 GHz. These good noise suppression capabilities are the most obvious results than that of two others. Thus, Co-Zr-Nb film is choose as a presentative in the mechanism study.

Among the three kinds of mechanisms introduced above, the classic magnetic shielding and FMR loss are related to permeability of the magnetic film, and the eddy current loss is related to applied frequency and the resistivity of magnetic film. Therefore, based on the original Co-Zr-Nb film, four assumed films with different permeability and resistivity were established in simulation. Separation between permeability property (including FMR) and film resistivity is investigated as shown in Table 3.1.

Film A has a constant permeability that the value is the same with that of Co-Zr-Nb film when frequency is 0.1 GHz. Therefore FMR loss is not existed in film A. The resistivity of film A is set to be infinite, in which there is no eddy current loss exists.

Film B has the same frequency dependent complex permeability as Co-Zr-Nb film. However it has an infinite resistivity that has no eddy current loss in the film.

Film C has two times of original permeability of Co-Zr-Nb film as shown as blue lines in Fig. 3.4. In film C, the value of permeability is higher although the FMR frequency is unchanged. It is expected to have higher FMR loss at the same FMR frequency. The resistivity of film C is the same with that of Co-Zr-Nb film, which means eddy current loss will generate inside the film.

Film D has the same frequency dependent complex permeability as Co-Zr-Nb film. However the resistivity is half value of that of Co-Zr-Nb film, which means it will have higher eddy current loss.

Table 3.1 Assumed film A to D

Film	Permeability, μ	Resistivity, ρ μΩ·cm
Co-Zr-Nb	$\mu_1(f)$	120
A	μ_1(0.1 GHz) = 630	∞
B	$\mu_1(f)$	∞
C	$2{\cdot}\mu_1(f)$	120
D	$\mu_1(f)$	60

3.3 Simulated results and discussion

3.3.1 Magnetic near field shielding

The simulated shielding effect of original Co-Zr-Nb film is shown as red solid line in Fig 3.4. The simulated result agrees with the measured result that shown as dotted line. It is noted that the validity of simulation was confirmed.

The simulated result of film A is shown as the blue broken line in Fig. 3.5. The result line is flat along with the frequency, showing a constant shielding effect. Only classical magnetic shielding is working because of the constant value of permeability it has. On the other hand, the red broken line shows the result of film B, which is slightly increase along with the frequency and has a little maximum peak at around 1 GHz. Then shielding effect is decreasing and there is a lowest dip at around 2 GHz. Because there is no eddy current loss existed, the gap between the results of film A and B at around 1 GHz is clarified to be the effect of FMR loss. Meanwhile, the gap between the results of film B and original Co-Zr-Nb film is considered the effect of eddy current loss. As the results, it is clarified that the frequency of maximum shielding is corresponded to the FMR frequency of magnetic film, while the eddy current loss dominates the value of shielding effect at FMR frequency.

Continually, the simulated result of film C is shown as black line in Fig. 3.5. The shielding effect of film C is about 3 dB higher than that of original Co-Zr-Nb film before 2 GHz. After 2 GHz, the shielding effect of film C is increased, which is about 6 dB larger than that of original Co-Zr-Nb film. As the results, higher permeability could lead to a better magnetic near field shielding effect.

Finally, the simulated result of film D is shown as green line in Fig. 3.5. In low

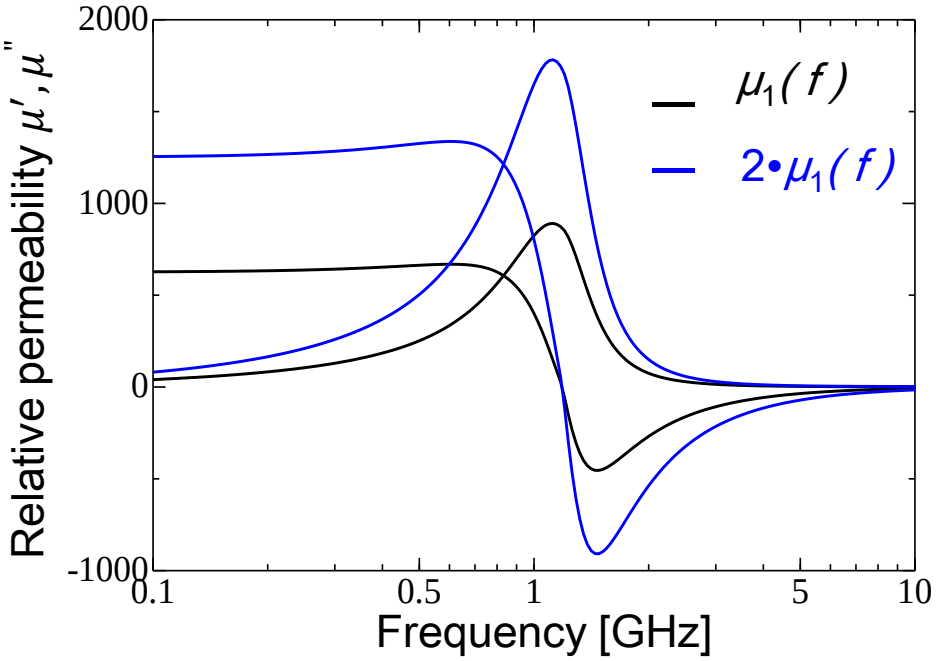

Fig. 3.4 Black lines: the original permeability of Co-Zr-Nb film. Blue lines: permeability that has twice value of that of Co-Zr-Nb film while FMR frequency is unchanged

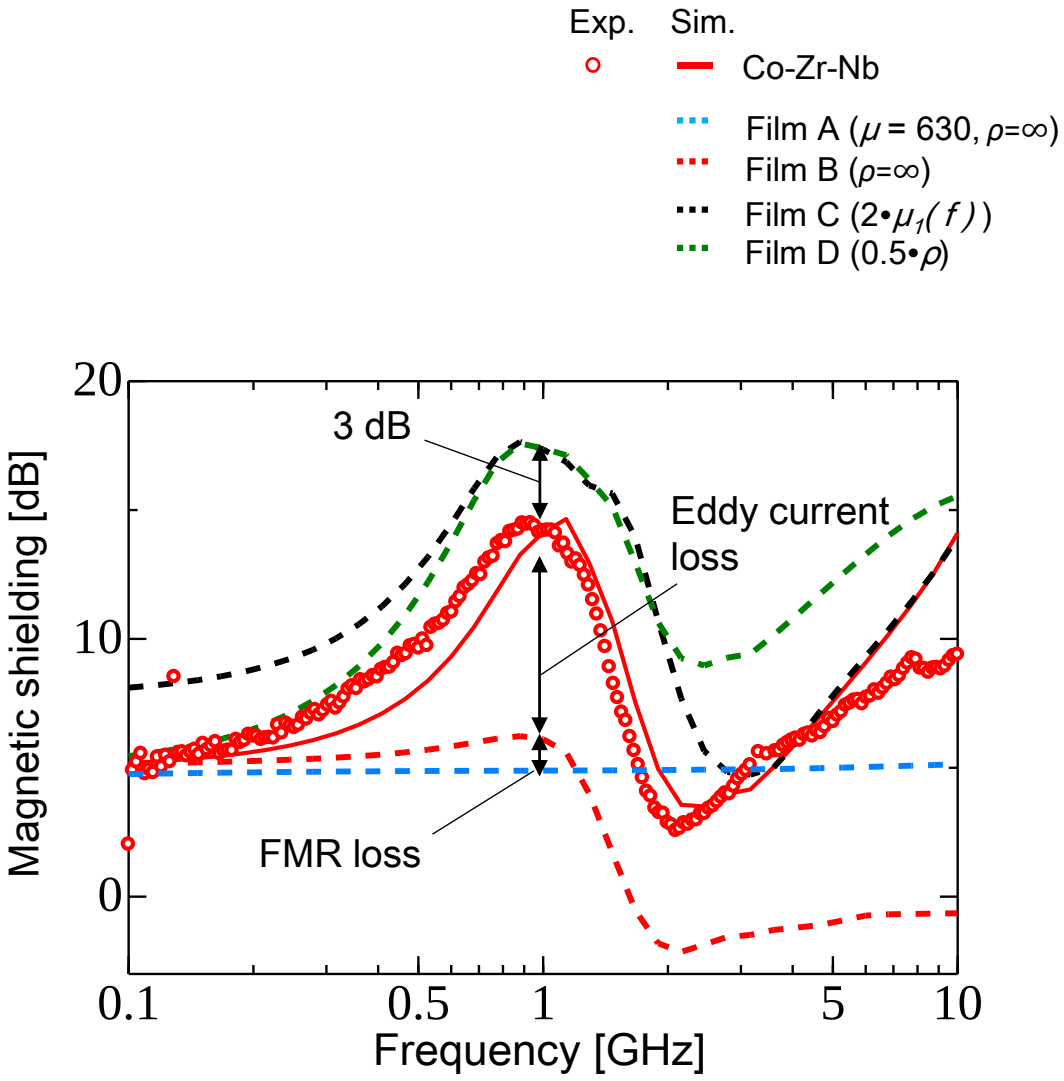

Fig. 3.5 Simulated shielding effect results of different assumed films with different permeability and resistivity.

frequency range, the shielding effect is similar with that of Co-Zr-Nb film. It is because of the same permeability leading to the same classical magnetic shielding. When the frequency increases, the shielding effect is increasing and about 3 dB higher than Co-Zr-Nb film at around FMR frequency 1.1 GHz. When the frequency is after about 3 GHz, the shielding effect is overlapped with the original simulated Co-Zr-Nb film. It explains that the eddy current loss is the main character in the last frequency range. As the results, it is shown that lower resistivity can provide higher eddy current loss and leads to a better magnetic near field shielding at FMR frequency.

3.3.2 Conductive noise suppression

Same as the previous chapter, the simulated conductive loss P_{loss}/P_{in} is shown as black solid line in Fig. 3.6. The simulated results also agree with the measurement results, which also provides the validity of the simulation.

The maximum peak of conductive loss is located at the frequency of 2.7 GHz, which is considered the result of demagnetization field. As shown in Fig. 3.7, when magnetic film was placed on the MSL, there is a demagnetizing field generated inside the film with an opposite direction of external magnetic field generated by signal line. This demagnetizing field could lead to a shift of FMR of magnetic film. As the calculation of FMR frequency

$$f_{FMR} = \frac{\gamma}{2\pi}\sqrt{\frac{M_s(H_k+N_dM_s)}{\mu_0}} \tag{3.11}$$

where f_{FMR} is FMR frequency, M_s is saturation magnetization, H_k is magnetic anisotropy field, μ_0 is permeability of vacuum, and N_d is the demagnetizing factor that

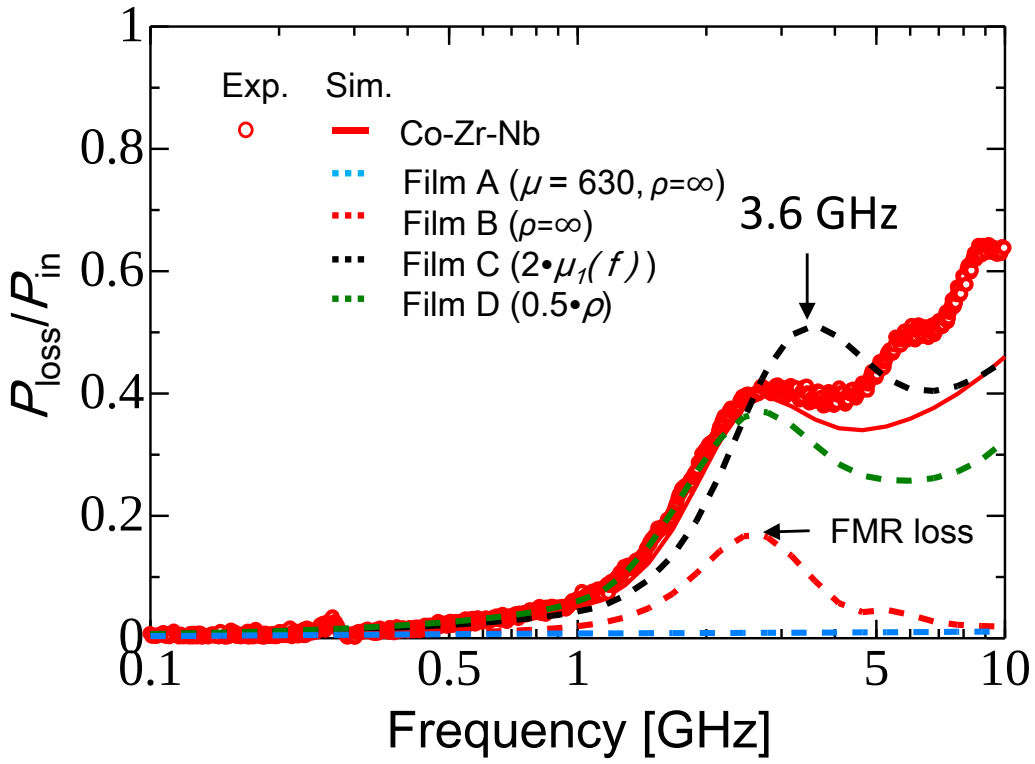

Fig. 3.6 Simulated conductive loss results of different assumed films with different permeability and resistivity.

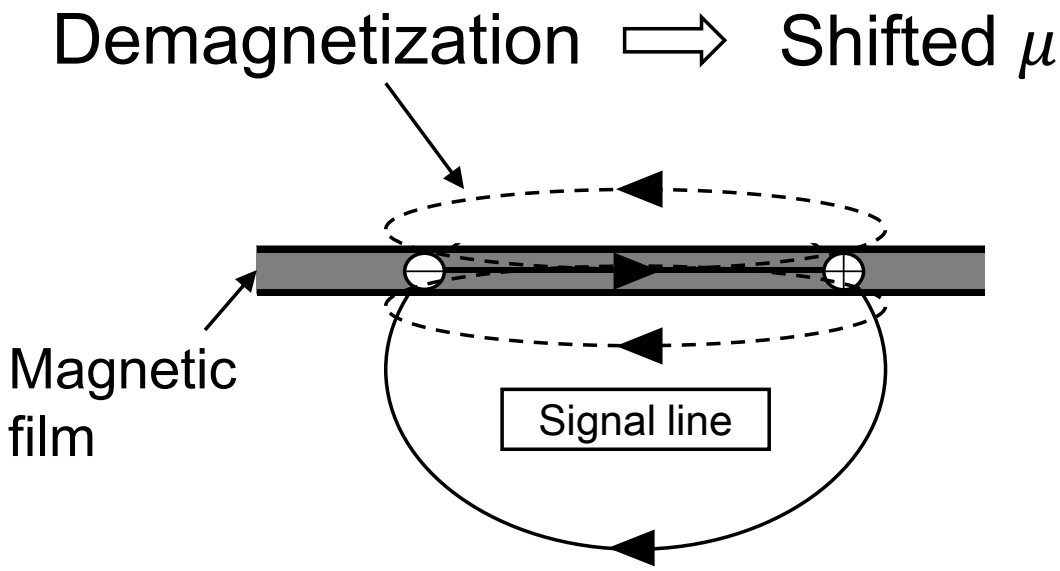

Fig. 3.7 Demagnetizing field that generates in the magnetic film with an opposite direction of applied magnetic field

is

$$N_d = \frac{t_m}{w_{eff}} = \frac{t_m}{w_s+\lambda} \tag{3.12}$$

where t_m is the thickness of magnetic film, w_s is the width of signal line, λ is the characteristic length of magnetic flux in the magnetic film. Characteristic length is defined as the distance from the edge of signal line to the place where the maximum magnetic field intensity becomes 1/e.

In this model that the film thickness is 1 μm, the width of signal line is 170 μm. Thus the demagnetizing factor is calculated as 5.88×10^{-3}. Finally, FMR frequency of formula (3.11) is calculated equal to 2.7 GHz, which is corresponded to the maximum of conductive loss as shown in Fig. 3.6. As a result, the mechanism of maximum conductive loss of magnetic film can be explained by the reason of demagnetizing field. In another word, the demagnetizing field leads to a shift of original FMR permeability to the higher frequency. In this case, the frequency of original permeability is shifted from 1.1 GHz to 2.7GHz and thus leads to the maximum of conductive loss at 2.7 GHz.

The calculation above is corresponded to the "shifted FMR" theory of reference [2], which proves the validity of it.

Based on the permeability and resistivity of original Co-Zr-Nb film, the simulated P_{loss}/P_{in} of film A to D are also shown in Fig. 3.6. The result of film A is shown as blue broken line, which is flat along with the frequency, showing not any of the loss existed inside the film because of the constant permeability and infinite resistivity.

The result of film B is shown as the red broken line, which is increased along with frequency and has a peak at around 2.7 GHz. After 2.7 GHz, the conductive loss is

decreased and finally becomes nearly zero. Because film B has the same frequency dependence of original Co-Zr-Nb film, and has infinite resistivity, it is shown that this peak is resulted by only FMR loss. Therefore, because eddy current loss is exponential growth with the increasing of frequency, the maximum conductive loss of Co-Zr-Nb film is considered the combination of FMR loss and eddy current loss.

The black broken line is the simulated result of film C, which has a twice value of original Co-Zr-Nb film and the same FMR frequency. The result line shows a peak at around 3.6 GHz, where the value is higher and the peak frequency is a little higher than that of Co-Zr-Nb film. The higher conductive loss is considered the result of higher imaginary part of permeability, which could have a higher FMR loss.

On the other hand, the higher value of permeability is brought by the increase of magnetic anisotropy field H_k, which will lead to an increase of shifted FMR frequency as shown in formula (3.11). Therefore, the higher frequency of maximum conductive loss is considered the result of higher magnetic anisotropy field H_k. Figure 3.8 (a) shows the different permeability of different magnetic anisotropy field H_k, where orange lines are the permeability of Co-Zr-Nb film, black broken lines are the permeability of twice value of Co-Zr-Nb film, and blue lines are another assumed film E, which is obtained by decreasing anisotropy field of film C, and thus FMR frequency is reduced from 1.1 GHz to 0.4 GHz. The simulated conductive losses of these three kinds of permeability are shown in Fig. 3.8 (b). The conductive loss of film E has a maximum value at around 2.7 GHz which is the same frequency as with that of Co-Zr-Nb film. Meanwhile, the loss degree is higher than that of Co-Zr-Nb film because of the higher imaginary permeability of film E. As a result, higher permeability can provide a better conductive loss, however it can lead to a shift of frequency of maximum loss. The decrease of magnetic anisotropy

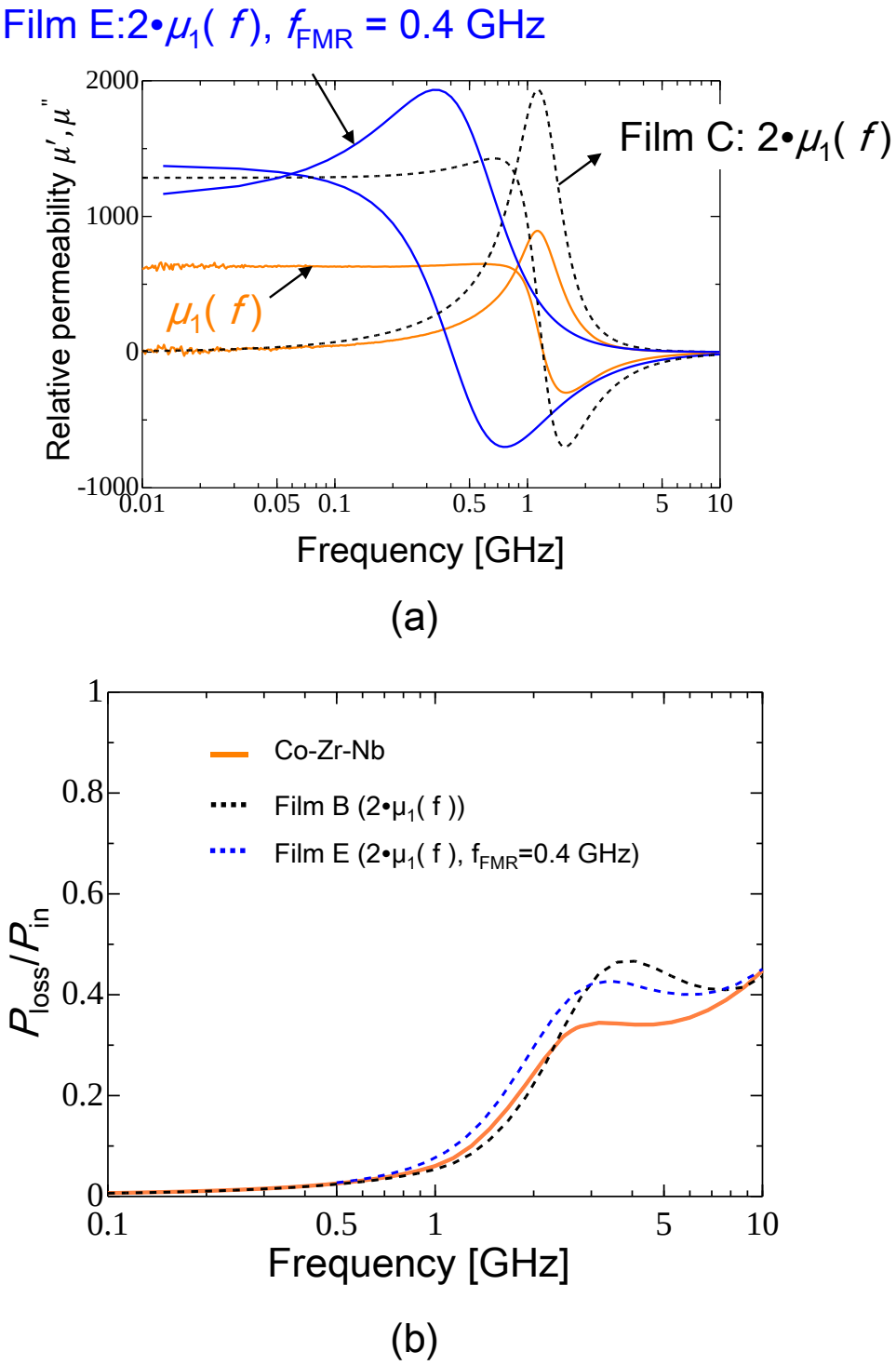

Fig. 3.8 (a) Additional film E that has a lower FMR frequency and the same value comparing to film C. (b) Conductive results of added film C comparing to the results of film C and original Co-Zr-Nb film

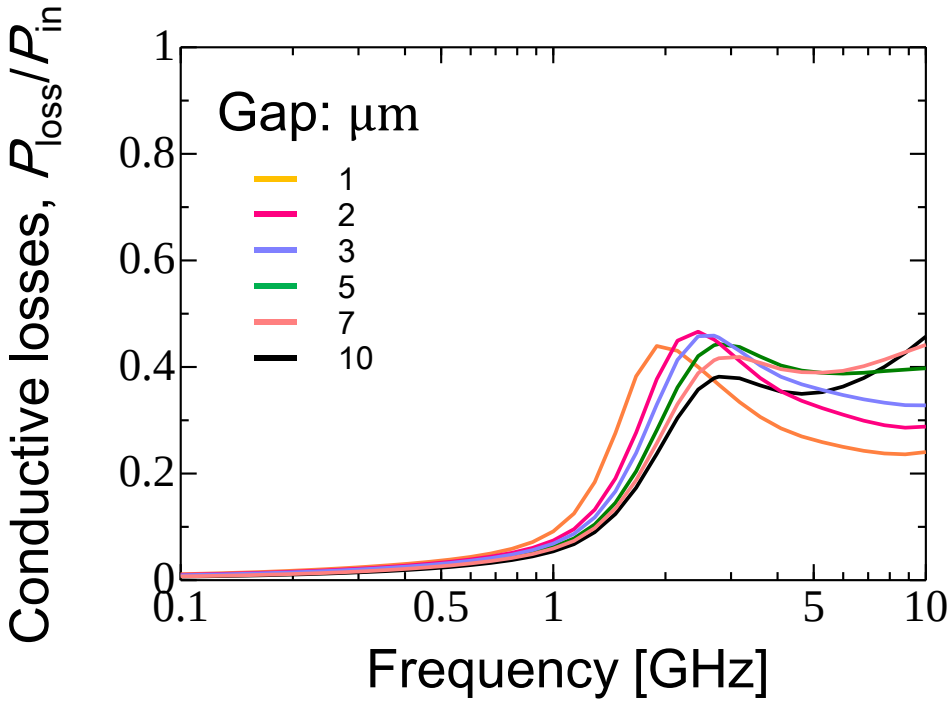

Fig. 3.9 Results of conductive loss of models that have different gap between magnetic film and signal line, from 1 μm to 10 μm

can bring the frequency of maximum loss back to the original place.

In the experiment, the distance between magnetic film and signal line is a rough estimation. The magnetic film is placed onto the surface of microtrip line directly and there are no accurate measurement about the gap between film and signal line. Furthermore, because the oxidation and roughness, the surface contact is irregular. Therefore, in the simulation based on Co-Zr-Nb film's characteristics, the same models with different gap distances were established and the conductive losses of them are shown in Fig. 3.9. In fig. 3.9, the black dotted line is the measured result while the rest cases are the simulated results with the gap distance from 1 μm to 10 μm.

As the results in Fig. 3.9, the frequency of maximum conductive loss is increased when the gap shifts from about 1.9 GHz to 2.7 GHz when the gap increases from 1 μm to 10 μm. As mentioned in the first part of this chapter, when the distance between magnetic film and signal line decreases, the distribution of magnetic field in the film is supposed to be expanded and thus leads to an increase of characteristic length. Then, the value of demagnetizing factor is decreased which causes the reduction of shifted FMR frequency.

And at the same time, the value of maximum conductive loss is increased when the gap distance increases from 1μm to 3 μm. After 3 μm, the value of maximum conductive loss is decreased with the increasing of gap distance. There is a peak conductive loss at the gap of 3μm.

3.4 Discussion of shielding effect and conductive loss

In chapter 2, the inductive and conductive noise suppression of magnetic film was measured at the same time and with a same frequency spectrum. It is easy for us to study

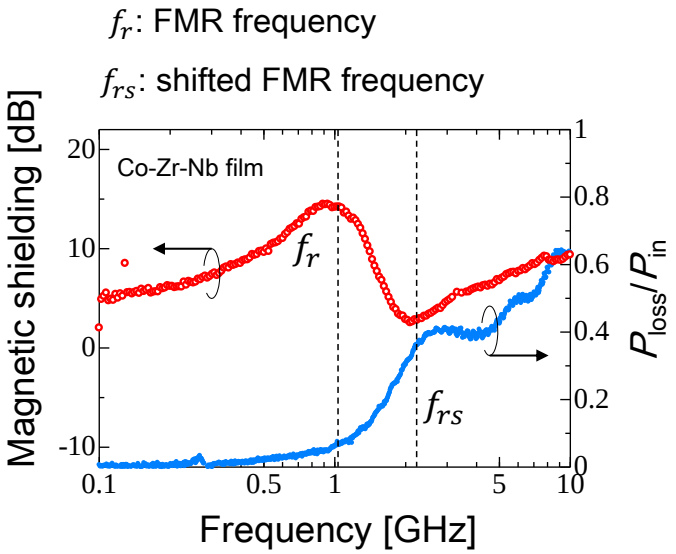

	Low f	f_r	f_{rs}
Shielding effect	High	Maximum	Low
conductive loss	Low	Low	High

Fig. 3.9 Shielding effect and conductive loss in the same frequency dependent.

the mechanism between the shielding effect and conductive loss at the same time. Fig. 3.10 puts both results of shielding effect and conductive loss of Co-Zr-Nb film together with the same frequency dependence.

First in low frequency, the shielding effect starts with 5 dB and increases with the frequency. Conversely, the conductive loss P_{loss}/P_{in} is close to zero. When the frequency comes to be from 1 GHz to 3 GHz, the shielding effect becomes maximum at 1 GHz and gradually decreases with the frequency, while the conductive loss gradually increases along with the frequency and has a maximum loss at around 2.7 GHz. The frequency of maximum conductive loss is corresponded to that of the minimum shielding effect. It is known that the shifted FMR frequency causes resonance and leads to the maximum absorption as conductive loss. Therefore, it is indicated that the minimum shielding effect at the same frequency is because of the shifted FMR and the resonance. Meanwhile, the description about the magnetic circuit resonance to the minimum shielding effect is discussed in Ref. [8].

3.5 Summary

In this chapter, first, based on the measurement in chapter 2, models in full wave electromagnetic simulations were established with the same dimension and structure. Co-Zr-Nb film was selected to be the representative in the mechanism study because of its obvious noise suppression effect. Then, the simulated results agrees with the experimental results. Thus, the validity of simulation was confirmed. Furthermore, different films with different permeability and resistivity were created in simulation, in order to study the contribution of permeability and resistivity of magnetic film to the shielding effect and conductive loss. As the results, it is clarified that the frequency of maximum shielding is

corresponded to the FMR frequency of magnetic film, while the eddy current loss dominates the value of shielding effect at FMR frequency. It is noted that twice value of permeability and half of resistivity could lead to an improvement of maximum shielding effect about 3 dB, respectively.

On the other hand, the maximum conductive loss is the results of shifted FMR frequency that affected by the demagnetizing field. It is indicated that twice value of permeability could obtain a higher conductive loss (+12 %) and a shift of maximum peak frequency. This shift is because of the increase of magnetic anisotropy field when obtain a higher value of permeability and keep FMR frequency unchanged.

The frequency of minimum shielding effect is near to the frequency of maximum conductive loss, where the generated magnetic circuit resonance is considered the reason and meanwhile at the same frequency the maximum absorption is happened.

References

[1] M. Sho, Y. Masahiro, “RF joule losses analysis in thin film noise suppressor estimated by 3-D equivalent circuit network,” IEEE Transactions on Magnetics, 2009, 45.10, pp. 4804-4807

[2] Muroga, S., Endo, Y., Mitsuzuka, Y., Shimada, Y., & Yamaguchi, M., “Estimation of peak frequency of loss in noise suppressor using demagnetizing factor,” IEEE Transactions on Magnetics, 2011, 47.2, pp. 300-303

[3] Shimada, Y., Ma, J., Ito, T., Yanagi, K., Endo, Y., Muroga, S., & Yamaguchi, M., “Performance of crossed anisotropy multilayered CoZrNb films as IC chip level electromagnetic noise suppressor. IEEE Transactions on Magnetics, 2014, 50.11, pp. 1-4

[4] K. Ohta, “磁気工学の基礎Ⅰ，Ⅱ(Basics of magnetics engineering Ⅰ，Ⅱ),” Kyoritsu Shuppan Co., Ltd., 1973

[5] Shimada, Y., “磁性材料―物性・工学的特性と測定法(Magnetic materials-physical properties, engineering characteristics and measurement method),” Kodansha, 1999

[6] Sumner, T. J., Pendlebury, J. M., & Smith, K., “Convectional magnetic shielding,” Journal of Physics D: Applied Physics, 1987, 20.9, 1095

[7] Shimada, Y., Shimoda, M., & Kitakami, O., “Multiple magnetic resonance in amorphous Co-Nb-Zr films with weak perpendicular anisotropy,” Japanese journal of applied physics, 1995, 34.9R, 4786

[8] Muroga, S., Asazuma, Y., Endo, Y., Shimada, Y., & Yamaguchi, M., “Analysis of magnetic flux through magnetic film with negative permeability,” IEEE Transactions on Magnetics, 2012, 48.11, pp. 4320-4323

Chapter 4
Study of crosstalk performance

4.1 Introduction

IC chips are highly integrated such that the space between the microstrip lines is preferred to be narrow. However, crosstalk between lines is recognized to be a significant issue in the design of IC chips, since the distance between lines is limited by the effect of crosstalk [1].

Through capacitive, inductive, and conductive coupling, the undesired effect generated from one line affects the normal signal transmission of another line. Consider a simple and representative model with two parallel lines having constant distance as shown in Fig. 4.1. The drive current that flows in line 1 (aggressor) generates capacitive and inductive couplings with line 2 (victim). In the capacitive coupling, the mutual capacitance C_m will lead to extra current $I_{\mathrm{near}}(C_{\mathrm{m}})$ in the near end and extra current $I_{\mathrm{far}}(C_{\mathrm{m}})$ in the far end. On the other hand, the mutual inductance will only lead to an extra current $I_{\mathrm{near}}(L_{\mathrm{m}})$ in the near end. These couplings are calculated as [2]

$$I_{near/far,\,C_m} = C_m \frac{dV_{driver}}{dt} \tag{4.1}$$

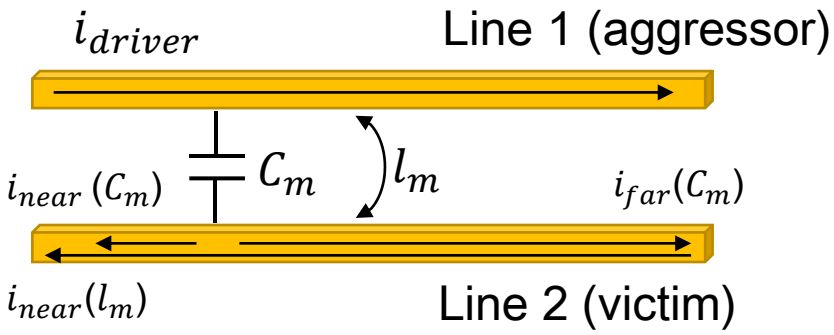

Fig. 4.1 Crosstalk between two paralleled lines

$$V_{near,L_m} = L_m \frac{dI_{driver}}{dt} \tag{4.2}$$

where, I_{driver} is the driver current that flows in line 1 (aggressor), $I_{\mathrm{near/far,\,C_m}}$ is the current generated by capacitive coupling in both near and far ends, $V_{\mathrm{near,\,L_m}}$ is the voltage generated by inductive coupling in only the near end.

Based on the four ports of the model shown in Fig. 4.1, the evaluation method for the crosstalk between two parallel lines is described as near-end crosstalk s_{31} and far-end crosstalk s_{41}.

The conventional methods related to crosstalk suppression are (1) structure design of signal line [3][4], (2) structure design of ground plane [5], and (3) the addition of guard traces between two signal lines [6]. Furthermore, another innovative idea has been proposed that magnetic material can provide crosstalk suppression to the printed circuit boards (PCBs). The magnetic composite (particles) were filled between two signal lines as shown in Fig. 4.2 (a) where the result shows the far-end crosstalk s_{41} is suppressed about 10-20 dB at the frequency of 1 GHz and the transmission coefficient s_{21} stays unchanged compared to the blank [7]. On the other hand, magnetic films [8] was deposited around the microstrip lines as shown in Fig. 4.2 (b), a 12 dB suppression of s_{41} was obtained here as well while the near-end crosstalk s_{31} showed no suppression results. However, these studies barely discuss the mechanism of crosstalk suppression in the aspect of magnetic properties.

In this study, based on the experimental results of crosstalk mentioned in chapter 2, first the mechanism of crosstalk suppression of magnetic films will be discussed in terms of permeability and resistivity. Next, when the magnetic film is placed on the signal lines as shown in Fig. 4.3, extra mutual inductance and capacitance will be generated.

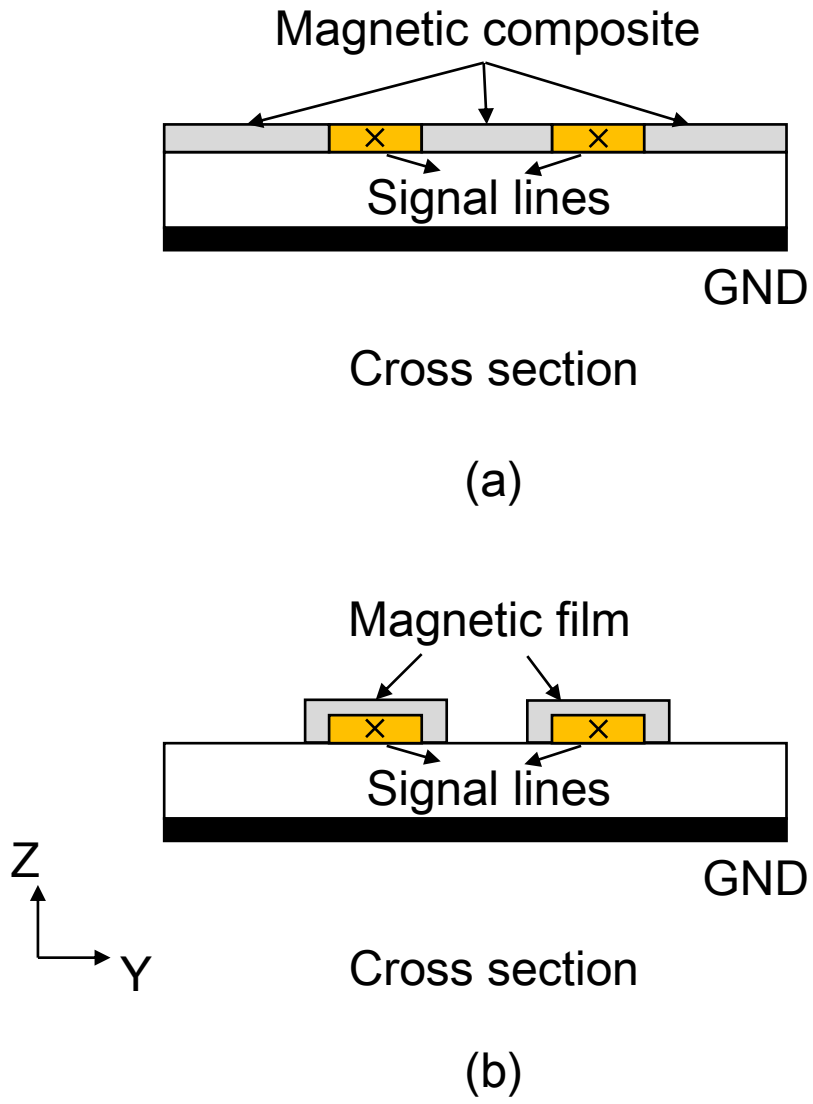

Fig. 4.2 Crosstalk suppression by magnetic materials, (a) magnetic composite (b) magnetic films

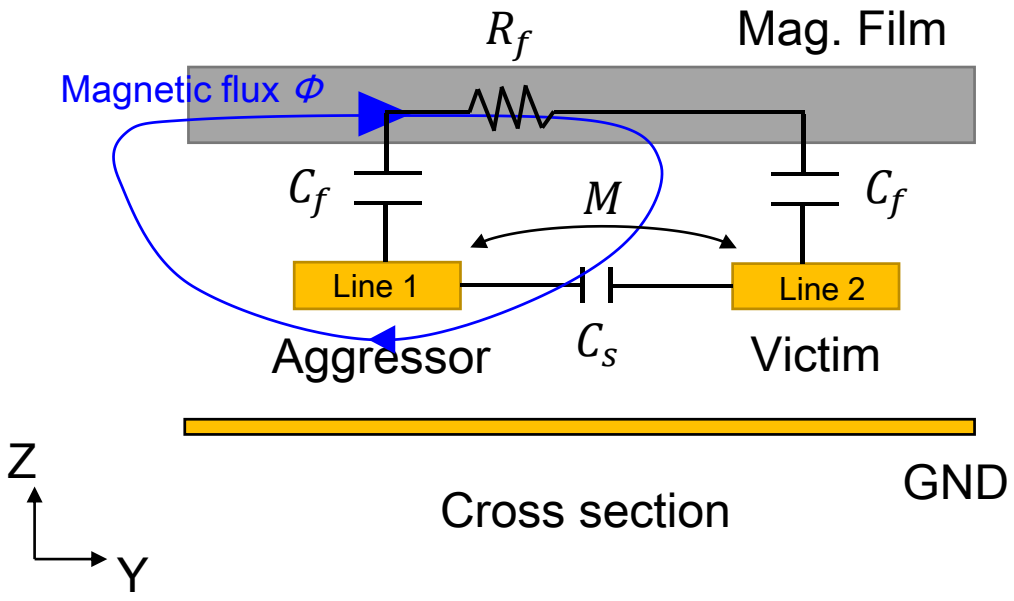

Fig. 4.3 Extra mutual capacitance and impedance generated by the cover of magnetic films on the signal lines.

as L_{f} and C_{f}. In order to quantitatively confirm the inductance influence of magnetic films and study the equivalent circuit of magnetic film-covered microstrip lines, the calculation of magnetic flux density inside the magnetic film in the cross section will be introduced.

Additionally, as per the experimental results mentioned in chapter 2, the Co-Zr-Nb film provides good near/far crosstalk suppression, as well as good shielding effect and conductive loss simultaneously. It is also selected as a representative example in the mechanism study in this chapter.

4.2 Discussion of permeability and resistivity

4.2.1 Simulation of crosstalk

Similar to the simulation method introduced in chapter 3, a model that has the same dimension and structure to the experiment was established. In the conditions of blank and film-covered, the simulated results of near and far-end crosstalk compared to the measurement results are shown in Fig. 4.4 (a) (b). This shows that the simulation results agree with the measurement results, which also confirms the validity of simulation.

As described in chapter 3, in order to study the mechanism of the magnetic film's crosstalk suppression, and to confirm the contribution of permeability and resistivity towards crosstalk suppression, additional three types of assumed films were created in the simulation. The permeability and resistivity are shown in table 4.1.

Film A has a constant permeability of vacuum i.e., μ_0. The resistivity of film A is the same value as that of the Co-Zr-Nb film. Film A has no permeability influence on crosstalk whereas only eddy current loss affects the result.

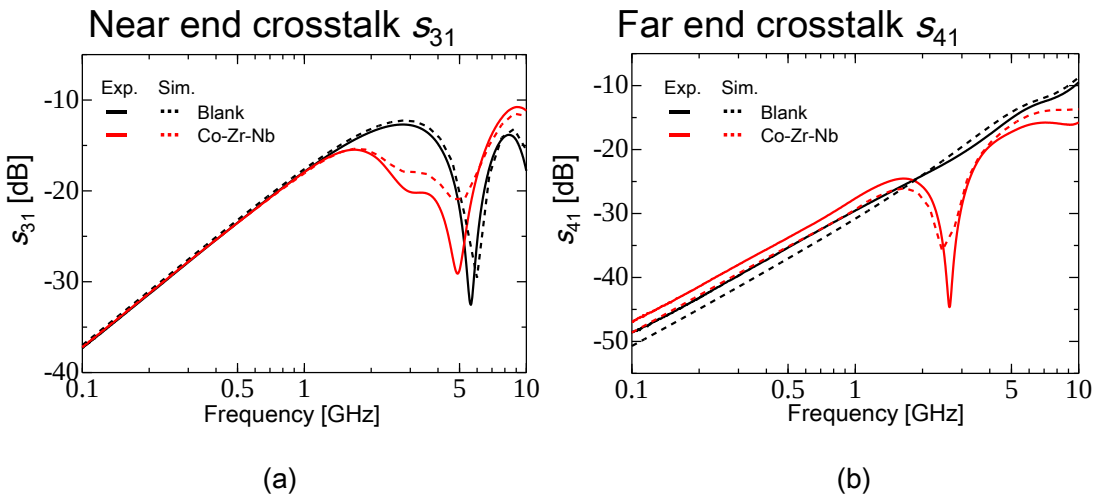

Fig. 4.4 Simulated results of crosstalk compared with those of measurement.

Table 4.1 Assumed film A to C

Film	Permeability, μ	Resistivity, ρ μΩ·cm
Co-Zr-Nb	$\mu_1(f)$	120
A	μ_0	120
B	$\mu_1(f)$	∞
C	$2\cdot\mu_1(f)$	120

Film B has the same permeability as that of Co-Zr-Nb film and an infinite resistivity. Thus, only permeability influence exists and eddy current loss is absent in film B, in contrast to film A. These two cases are aimed to separate the FMR loss and eddy current loss in order to clarify their individual contribution.

Film C's permeability is twice the value of permeability of the Co-Zr-Nb film while the FMR frequency does not change and is the same as shown by the blue line in Fig. 3.4. The resistivity is the same value as that of the Co-Zr-Nb film. This case is aimed to check the quantitative relationship between the numerical value of permeability and crosstalk suppression.

4.2.2 Mechanism discussion of permeability and resistivity

The simulated results of each assumed film A to C and the original Co-Zr-Nb film are shown as the broken lines in Fig. 4.5. The solid lines are measurement results that were already shown in chapter 2.

(1) Near-end crosstalk s_{31}

The measurement and simulation results of near-end crosstalk s_{31} are shown in Fig. 4.5 (a) with the frequency from 0.1 GHz to 10 GHz. In low frequency, the lines of film-covered cases overlap with those of blank, indicating that the covering of the magnetic film is not effective to near-end crosstalk in the low frequency. However, in the frequency of 1 GHz to 10 GHz, the effect of magnetic films is obvious as shown in the enlarged figure of (b).

Firstly, the result of film A where no permeability effect exists in the film is shown as a green broken line. It has an only large dip at around 5.5 GHz, which is similar to the result of blank. The LC resonance is considered to be the reason. The dip-frequency of

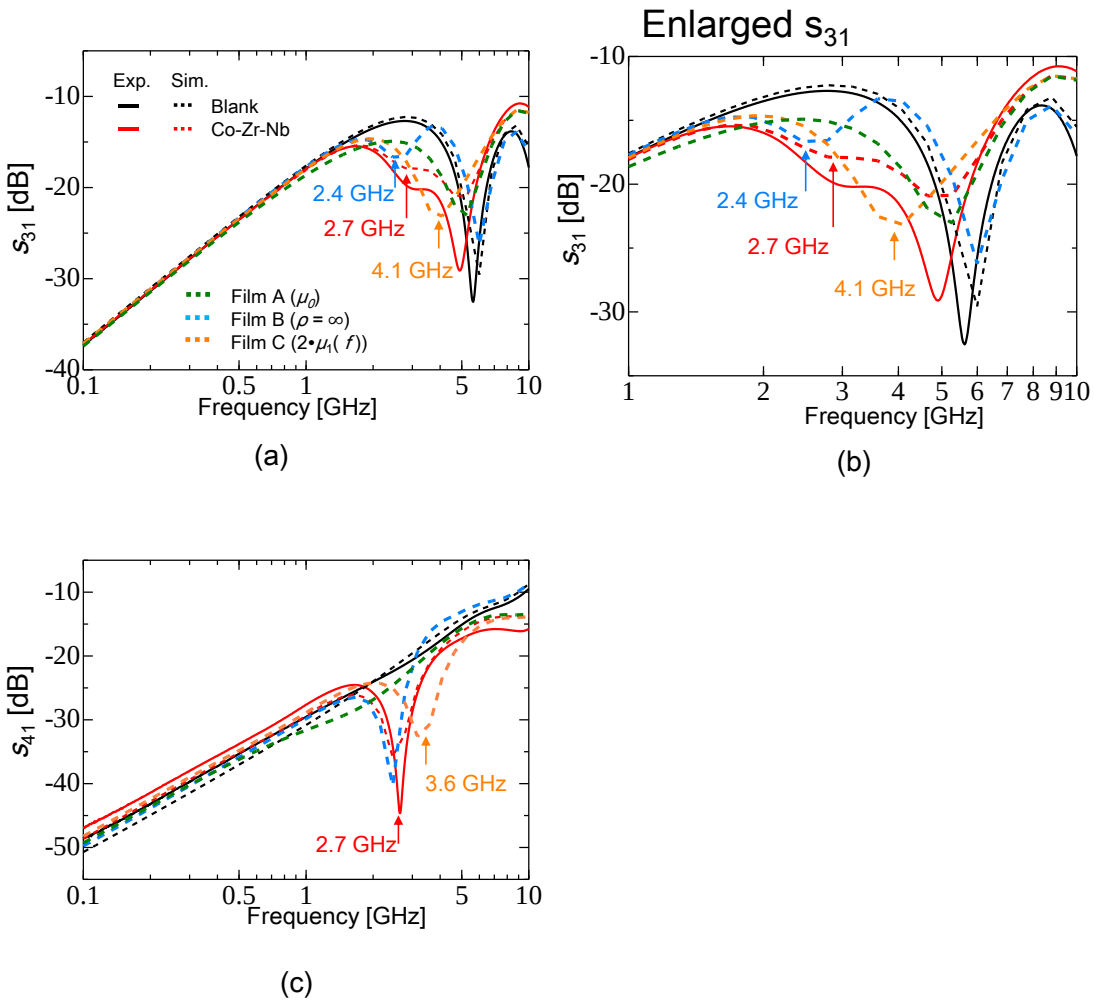

Fig. 4.5 Crosstalk results of assumed films A to C, (a) near-end crosstalk, (b) enlarged representation of near-end crosstalk in frequencies from 1 GHz to 10 GHz, (c) far-end crosstalk

film A is slightly shifted towards lower frequencies than that of blank. This is recognized as the effect of resistivity on the capacitance of the whole model. A similar result is obtained in the measurement result of the Co-Pd film as shown in chapter 2 Fig. 2.7 (a). As a result, when the value of permeability is low, there is little effect of permeability on crosstalk performance.

Secondly, the result of film B where no eddy current loss exists in the film is shown as a blue broken line. In addition to the dip at around 6 GHz, there is another dip at around 2.4 GHz. Owing to the frequency dependence of permeability that film B has, this dip is considered to be the result of FMR. Comparing the simulated result of the original Co-Zr-Nb film, shown as a red broken line, the dip of film B is shifted towards lower frequency, which ranges from 2.7 GHz to 2.4 GHz. This difference is considered to be the reason for eddy current. As a result, it is indicated that the dip of the Co-Zr-Nb film that has a near-end crosstalk suppression about 7 dB at around 2.7 GHz as a result of FMR.

Finally, the result of film C that has twice value of permeability and the same resistivity of the Co-Zr-Nb film is shown as an orange broken line. Similar to film A, only one dip exists for film C, however this dip occurs at around 4.1 GHz. Therefore, the dip of film C is considered to be the result of both FMR and eddy current. On the other hand, the value of the dip is larger than that of the original Co-Zr-Nb film and film B, which shows that the high value of permeability may lead to a better near-end crosstalk suppression.

(2) Far-end crosstalk s_{41}

The measurement and simulation results of far-end crosstalk s_{41} are shown in Fig. 4.5 (c) with frequencies from 0.1 GHz to 10 GHz. In the low frequency range before 1 GHz, the results of film-covered microstrip lines are slightly higher (about 3 dB) than those of

blank, which shows that the covering of magnetic film will causes a slight increase in far-end crosstalk at low frequencies. In the frequencies above 1 GHz, dips are generated when each of magnetic films are placed on the signal line.

First, the result of film A that has the permeability of vacuum and the same resistivity as that of the Co-Zr-Nb film has a flat depression in the frequency range of 1–4 GHz. This is because of the resistivity, which is similar to the measurement result of Co-Pd granular film as shown in Fig. 2.7 (b).

Then, the result of film B is shown as a broken blue line such that no eddy current loss exists in the film. One dip occurred at around 2.4 GHz that indicates this dip is not the result of LC resonance, rather the result of FMR of the magnetic film. The frequency at which the dip occurred is a slightly smaller than that of the original Co-Zr-Nb film, which is considered to be the result of resistivity difference. In other words, this small shift of frequency is affected by the capacitance change.

Finally, the result of film C that has twice value of permeability and the same resistivity of the Co-Zr-Nb film is shown as an orange broken line. Owing to the similar frequency dependence of permeability that has the same FMR frequency, this result has a dip at around 3.6 GHz. Compared with the result of the Co-Zr-Nb film, the dip-frequency of film C is higher than that of the Co-Zr-Nb film; this the mechanism is considered to be the same as that mentioned in the result of $P_{\mathrm{loss}}/P_{\mathrm{in}}$.

In the results of the original Co-Zr-Nb film and film B, the frequency of dips that resulted by permeability in s_{31} is the same as that of s_{41}. As maximum conductive loss is considered to be the reason for the shifted FMR frequency leading to maximum energy absorption, it is indicated that the mechanism of these dips may also be explained by the shifted FMR frequency. On the other hand, in the results of film C, the dip-frequency of

s_{31} (at 4.1 GHz) is different with that of s_{41} (at 3.6 GHz). The frequencies corresponding to dips between s_{31} and s_{41} in the results of the Co-Zr-Nb film and film B proves that the dips of s_{31} at 4.1 GHz are the overlap result of FMR permeability and LC resonance.

4.2.3 Demonstration of FMR influence to crosstalk suppression

Another demonstration has been carried out in order to confirm whether the dips in crosstalk are related to the FMR permeability of magnetic film. Fig. 4.6 shows an experimental setup where a magnet was placed beside the paralleled signal lines. The magnetic field generated by the magnet flows approximately vertically through the longitude of the signal line, and the direction of this magnetic field is also vertical to the easy axis of the magnetic film. The distance between the magnet and magnetic film is designed from 23 mm to 35 mm; closer the distance between them, stronger the magnetic field added to the film.

With the cover of three types of different magnetic films mentioned in chapter 2, the measurement results of magnetic field added crosstalk is shown in Fig. 4.7.

(1) In the results of the Co-Zr-Nb film, when the magnet is brought close, the original dips in near and far-end crosstalk at 2.7 GHz are shifted to a lower frequency and finally disappear when the distance is lower than 23 mm. (2) In the results of the Co-Pd granular film, the curves nearly overlap when the distance changes, and the movement of magnetic moments does not affect the crosstalk performance. The low value of permeability is considered to be the reason. (3) In the results of the Ni-Fe magnetic film, the near-end crosstalk at varying distances are nearly the same while in the results of far-end crosstalk, a similar tendency occurs as that observed in the Co-Zr-Nb film.

Therefore, the mechanism may be explained as such; when the magnet is closer, the

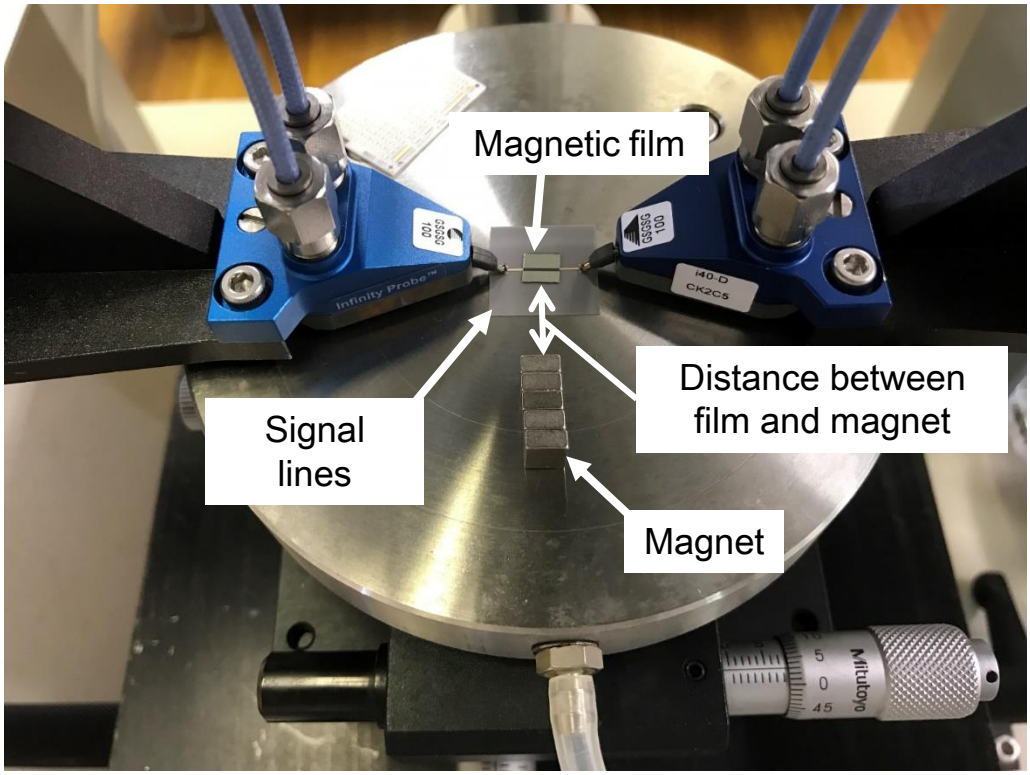

Fig. 4.6 Demonstration related to the influence of FMR property on crosstalk suppression

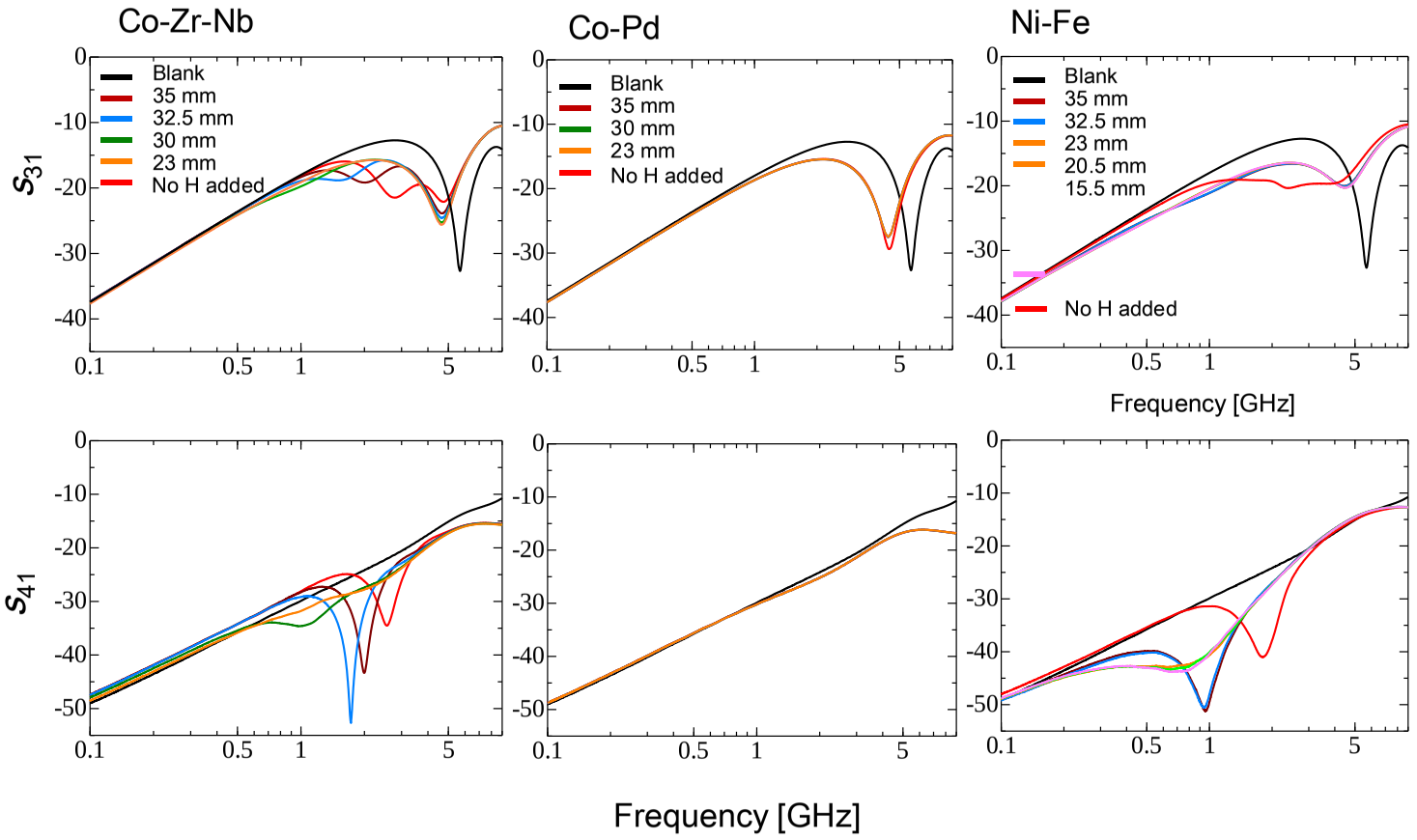

Fig. 4.7 Crosstalk results when a magnet is placed beside the magnetic film

added ambient magnetic field becomes stronger, which makes the magnetic moment gradually move towards the direction of the added magnetic field. Finally, when the magnet becomes closer to the film, the added magnetic field becomes stronger and reaches saturation. Therefore, the phenomenon of FMR property vanishes and the dips of crosstalk gradually disappear.

4.3 Calculation of magnetic flux density inside magnetic film through characteristic length

4.3.1 Theoretical calculation of magnetic flux density

As mentioned in the introduction part of this chapter, in order to quantitatively confirm the inductance influence of magnetic film and study the equivalent circuit of magnetic film-covered microstrip lines, the calculation of magnetic flux density inside the magnetic film in the cross section is necessary to be analyzed.

According to Ref. [9], a circle in the cross section around the signal line is created as shown in Fig. 4.8. For each of the lines 1, 2, 3, and 4, a corresponding formula is established based on Ampere's law,

$$H_1 \Delta l_1 = \frac{\phi \Delta x}{w \mu_0 \mu_1 t_1} \tag{4.3}$$

$$H_2 \Delta l_2 = \frac{g_a}{w \mu_0} \frac{d\phi(x)}{dx} \tag{4.4}$$

$$H_3 \Delta l_3 = \frac{\phi \Delta x}{w \mu_0 \mu_2 t_2} \tag{4.5}$$

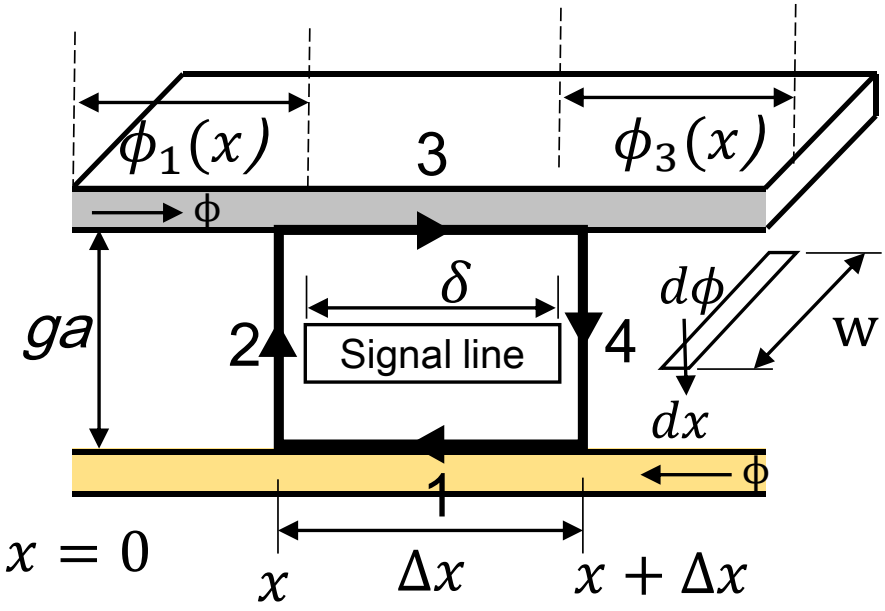

Fig. 4.8 Cross section of microstrip lines covered by a magnetic film, magnetic field is calculated based on circle the 1234 through Ampere's law

$$H_4 \Delta l_4 = -\frac{g_a}{w\mu_0}\frac{d\phi(x+\Delta x)}{dx} \tag{4.6}$$

where H_a (hereafter a = 1–4) is the magnetic field, Δl_a is the variable length of the magnetic circle, ϕ is the magnetic flux, Δx is the variable length in the cross section, w is the length of magnetic film, μ_0 is the permeability of vacuum, μ_1 and t_1 are the relative permeability and thickness of dielectric layer SiO_2 between the signal line and ground, respectively. Similarly μ_2 and t_2 are the relative permeability and thickness of the magnetic film, respectively, g_a is the distance between the magnetic film and dielectric layer.

Then, the total current I is calculated as the integral of (4.3)–(4.6)

$$\oint Hdl = i = \frac{\Delta x}{\delta} I \tag{4.7}$$

where δ is the width of signal line. The general solution of (4.7) is shown as

$$\phi_3(x) = A_1 e^{\frac{x}{\lambda}} + A_2 e^{-\frac{x}{\lambda}} \tag{4.8}$$

where $\phi_3(x)$ is the distance dependence of magnetic flux inside the magnetic film. x is the distance from the edge of the signal line to infinity. A_1 and A_2 are constant values determined by boundary conditions. The final solution is transferred to magnetic flux density divided by area S as

$$B(x) = B_0 e^{-\frac{x}{\lambda}} \tag{4.9}$$

where λ is defined as the characteristic length, which is the distance from the edge of the

signal line to the place where the magnetic flux intensity becomes 1/e, as shown in Fig. 4.9. It is calculated as

$$\lambda = \sqrt{\frac{g_a}{\frac{1}{\mu_1 t_1}+\frac{1}{\mu_2 t_2}}} \tag{4.10}$$

4.3.2 Result of characteristic length

Based on (4.10), the calculated result of characteristic length λ is shown in Fig. 4.10. The real part of λ becomes greatest at 2.7 GHz, and then gradually reduces to 0. In contrast, the imaginary part of λ becomes least at 3.0 GHz, implying that it dominates in the magnetic flux distribution at frequencies greater than the FMR frequency.

In this calculation, the demagnetizing field is considered, and thus, the shifted FMR frequency is included in the results. Furthermore, in (4.10), μ_2 is the complex permeability of the magnetic film, which is shown in Fig. 3.3. The FMR frequency is located at around 1.1 GHz while the peak value of λ is at 2.7 GHz. This indicates that λ shifts to higher frequencies owing to the demagnetizing field.

4.3.3 Result of distribution of magnetic flux density B

The result of λ can be speculated in the alternated distribution of the B vectors and the attenuated value of B along the increasing distance, as shown in Fig. 4.11 (a). To verify these speculations quantitatively, the B vector of the magnetic flux density and B distribution inside the magnetic film in the cross-section were estimated through the simulation and characteristic length analysis (Eq. (4.9), as shown in Fig. 4.11(b) and (c), respectively). They show the results of the instantaneous value of B when B is maximum at x = 0 for the frequency of 2.7 GHz.

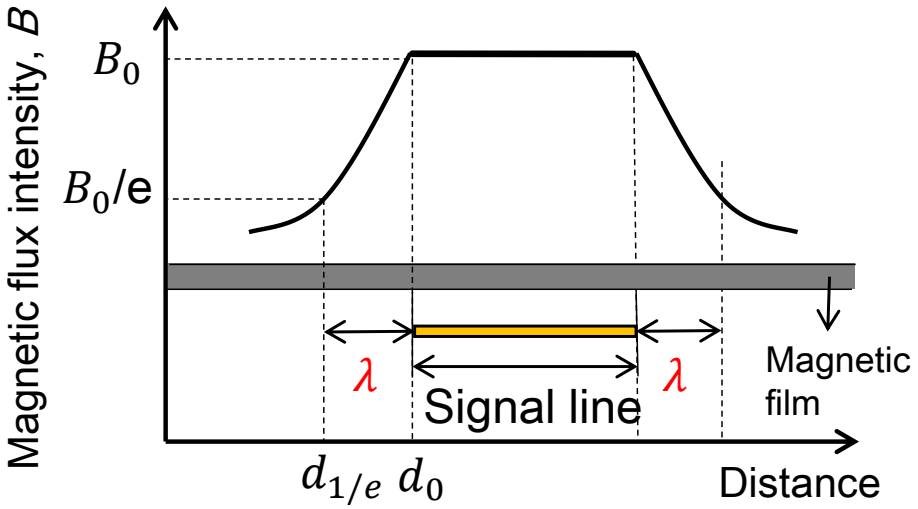

Fig. 4.9 Assumed distribution of magnetic field inside the magnetic film in the cross section. Characteristic length λ is the distance from the edge of the signal line to the place where the magnetic flux intensity becomes 1/e.

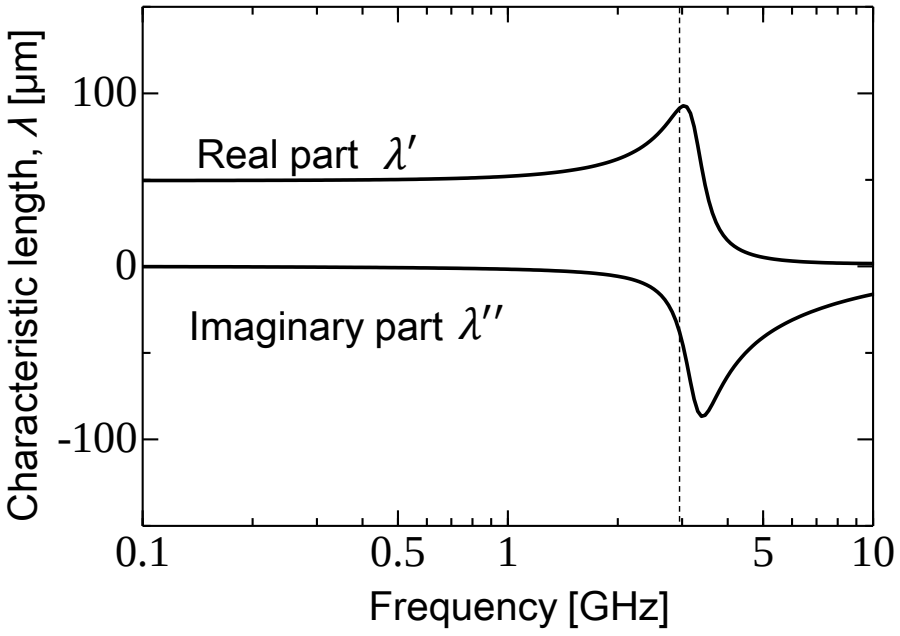

Fig. 4.10 Calculated result of the frequency dependence of characteristic length that has a real part and an imaginary part

Fig. 4.11 (b) is the simulated result of B vectors distribution in the cross section. As it is observed, the orientation of B vectors is concentrated and distracted alternately along the distance. The value of B is also attenuated and decreased along the distance.

Fig. 4.11 (c) is the calculated result of (4.9), which shows that the value of B decreases along the distance and exists an intersection point with zero axis (around 420 μm), corresponding to the place comprising the B vector concentration in Fig. 4.11 (b). The value then decreases negatively, oscillates weakly, and gradually becomes null as the distance from the signal line edge increases. In case of the distance of less than 200 μm, the characteristic length analyzed result almost agrees with the simulation result, and thus satisfactorily explains the B vector distribution in Fig. 4.11 (b). However, in the cases of distances greater than 200 μm, the analyzed characteristic lengths and simulated results differ slightly; this may be ascribed to either the influence of the local demagnetizing field and/or calculation accuracy.

Hence, the magnetic flux density distribution inside the magnetic-film-type noise suppressor could be quantitatively estimated by calculating the characteristic length. Magnetic flux density is distributed like “magnetic poles” in the cross section of the magnetic film. It may assist in the evaluation of inductance coupling in future works.

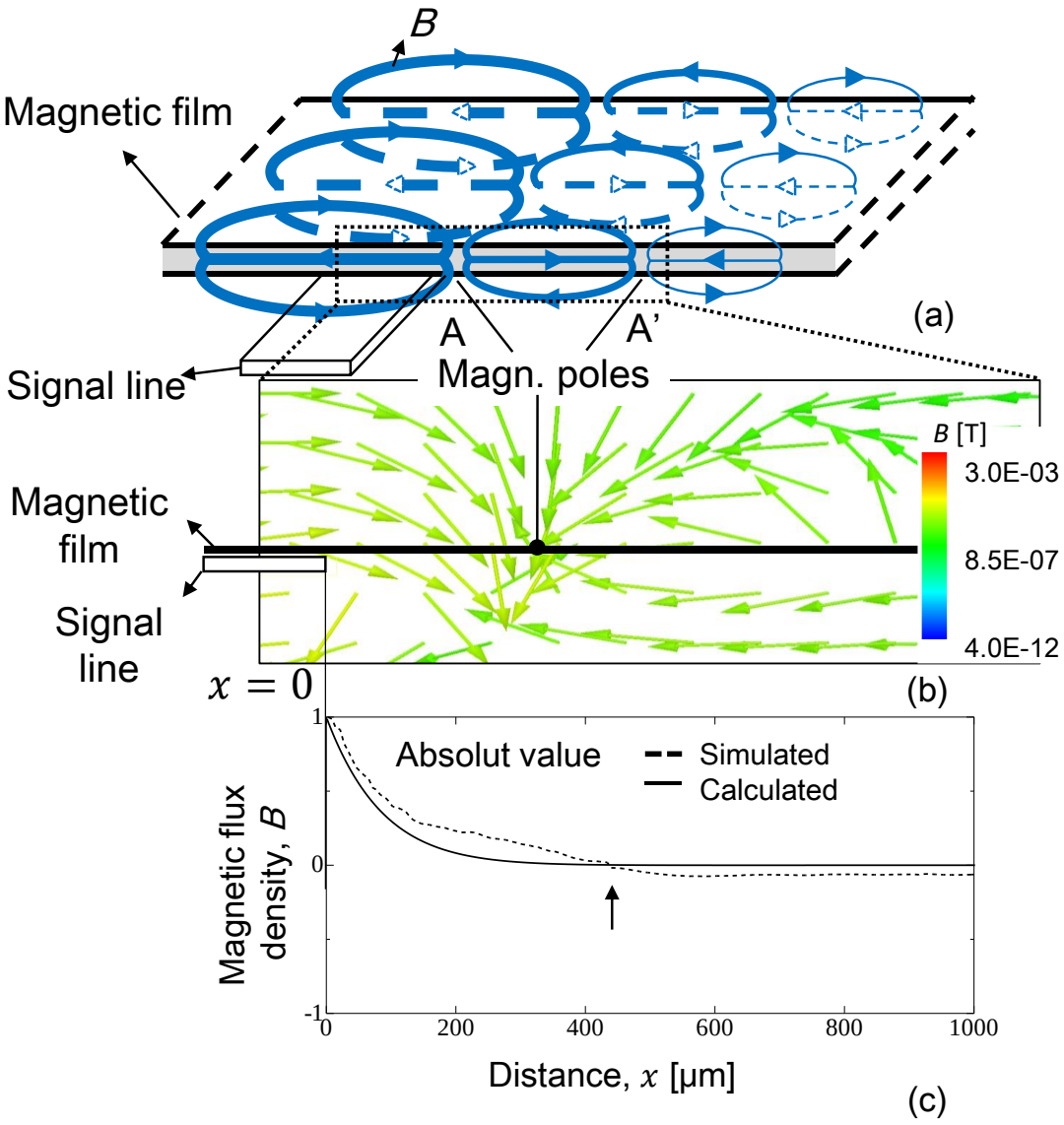

Fig. 4.11 (a) Distribution of magnetic flux density inside the magnetic film, (b) simulated result of magnetic vector distribution, (c) distance dependence of magnetic flux density: results of simulation and calculation.

4.4 Summary

In this chapter, first, the capability of crosstalk suppression of magnetic films is confirmed. The simulated results agree with the experimental results. The dip-frequencies in near and far-end crosstalk correspond to the maximum conductive loss of the magnetic film. The mechanism of dips in near and far-end crosstalk is due to the maximum absorption and shifted FMR frequency.

Second, through the calculation of the characteristic length, the distribution of magnetic flux density inside the magnetic film was clarified numerically. The results demonstrated that the complex permeability of the magnetic film leads to a complex characteristic length, thus resulting in the formation of distributed magnetic poles along the film width. In addition, the results show that these distributed magnetic poles must be considered in terms of inductive crosstalk and conduction loss in the design of patterned magnetic-film-type noise suppressors. Furthermore, the inductance coupling of the magnetic film may be clarified based on the results of magnetic flux density distribution.

Based on these results, this study may aid the quantitative evaluation of crosstalk between the aggressor and victim lines in the design of the patterned magnetic-film-type noise suppressors.

References

[5] Sharawi, Mohammad S., “Practical issues in high speed PCB design,” IEEE Potentials 23.2, 2004, pp. 24-27

[6] Clayton R. Paul, “Transmission Lines in Digital and Analog Electronic Systems: Signal Integrity and Crosstalk,” Copyright © 2010 John Wiley & Sons, Inc., 2011

[7] Wu, J. J., Chiueh, H. L., Chang, C. C., Yi, C. F., Kao, Y. H., & Yang, T. J., “A new type of differential transmission lines with surface plasmon polaritons in microwave regime,” Progress in Electromagnetics Research Symposium-Fall (PIERS-FALL), IEEE, 2017

[8] W. Boping, and T. Mo, “Barbed transmission lines for crosstalk suppression,” Electromagnetic Compatibility (APEMC), 2012 Asia-Pacific Symposium on. IEEE, 2012

[9] Leong, K. M., Guyette, A. C., Elamaran, B., Shiroma, W. A., & Itoh, T., “Coupling suppression in microstrip lines using a bi-periodically perforated ground plane,” IEEE microwave and wireless components letters 12.5, 2002, pp. 169-171

[10] Huang W., Chi-Hao L., and Ding-Bing L., “Suppression of crosstalk using serpentine guard trace vias,” Progress In Electromagnetics Research 109, 2010, pp. 37-61

[11] Kayama, S., Sonehara, M., Sato, T., Yamasawa, K., & Miura, Y., “Cross-talk suppression in high-density printed circuit boards using magnetic composite filled in spacing between signal lines,” IEEE Transactions on Magnetics 45.10, 2009, pp. 4801-4803

[12] M. Sonehara, S. Kayama, T. Sato, K. Yamasawa, Y. Miura., “Suppression of Crosstalk in High-density Printed Circuit Boards by Coating Electroless-plated Ni-P Alloy Film on Signal Lines,” J. Magn. Soc. Jpn., 35.2, 2011, pp. 82-87

[13] R. Jones, “Analysis of the efficiency and inductance of multiturn thin film magnetic recording head,” IEEE Transactions on Magnetics, vol. 14, 1978, pp. 509-511

Chapter 5
Conclusion

5.1 Summary

In this thesis, a model of a magnetic film placed on a microstrip line was established in order to simplify the complicated film-covered IC chip design. Inductive, conductive, and crosstalk noise suppression capabilities of three different magnetic films were measured by the proposed method. The mechanism studies were carried out by creating a same model as that of the experiment in a 3-dimension full wave electromagnetic simulator. All the results may aid in completing the design guidelines of magnetic film-type noise suppressors used in IC chips.

The content of each chapter is summarized below.

In chapter 2, a method that can evaluate both inductive and conductive noise suppression capability of magnetic films was proposed. Thereby, the magnetic shielding effect, conductive loss, and crosstalk suppression of three types of magnetic films were measured. The most obvious shielding effect and conductive loss were in the case of the Co-Zr-Nb film, in which the frequency corresponding to the maximum shielding effect and maximum conductive loss were different. Furthermore, it shows that minimum

shielding occurred at the frequencies where the conductive loss became the highest.

In chapter 3, a model with the same structure and dimension of the experiment was created in a 3-dimension full wave electromagnetic simulator, in order to study the contribution of permeability and resistivity on the shielding effect and conductive loss. In the results, the maximum shielding effect corresponded to the FMR frequency while the maximum conductive loss corresponded to the shifted FMR frequency. The shift of FMR frequency is considered to be the result of demagnetizing field that is generated inside the magnetic film in the opposite direction to the magnetic field generated by the signal line.

The frequency of maximum near-field shielding is dominated by the FMR frequency. Doubling the permeability and halving the resistivity improves the shielding effect by about 3 dB. It is because higher permeability provides better concentration of magnetic flux, and lower resistivity increases the eddy current loss. In addition, the frequency of maximum conductive loss is dominated by the shifted FMR frequency, where the FMR loss becomes the greatest. In the shifted FMR frequency, the magnetic near-field shielding becomes the lowest owing to the magnetic circuit resonance.

In chapter 4, the magnetic film provides good crosstalk suppression in particular frequencies. Except for the LC resonance, the dip-frequencies in crosstalk agree with the calculated shifted FMR frequency. Mechanism study of the crosstalk suppression of magnetic films was conducted in order to clarify the contribution of permeability and resistivity on crosstalk suppression. The results show that there are dips in both near and far-end crosstalk, where the dip-frequencies corresponded to those of maximum conductive loss. It is concluded that the shifted FMR frequency is the reason for these dips in the crosstalk results.

In conclusion, first, the contributions of the magnetic materials' individual permeability

and resistivity were clarified quantitatively. Then, the interaction between shielding effectiveness and conductive loss was confirmed in the same frequency spectrum. Finally, the crosstalk performance of each type of magnetic film and the corresponding mechanism were confirmed. The obtained results may contribute towards the design of magnetic film-type noise suppressors in IC chips.

5.2 Outlook

Currently, the magnetic films discussed are only a small part of the entire magnetic family. The composition of different types of materials, including non-magnetic materials, is expected to have higher permeability and lower resistivity. Magnetic materials with metals such as copper and different fabrication methods are desired to obtain better flexibility. Magnetic compositions with non-magnetic materials such as carbon are expected as well to obtain better corrosion resistance.

In addition, for the further study of crosstalk suppression capability, the calculation of the distribution of magnetic flux density inside the magnetic film is the first step. An equivalent circuit is necessary in order to investigate the changes of mutual inductance and capacitance brought about by the use of magnetic films.

Appendix

A. Publications

[1] Ma, J., Muroga, S., Endo, Y., Hashi, S., Yokoyama, H., Hayashi, Y., Ishiyama, K., “Analysis of magnetic film-type noise suppressor integrated on transmission lines for on-chip crosstalk evaluation,” IEEE Transactions on Magnetics, 54.6: 1-4, 2018 (Chapter 4)

[2] Ma, J., Muroga, S., Endo, Y., Hashi, S., Naoe, M., Yokoyama, H., Hayashi, Y., Ishiyama, K., “Noise suppression and crosstalk analysis of on-chip magnetic film-type noise suppressor," AIP Advances 8, 056613, 2018 (Chapter 2,3)

[3] Ma, J., Aoki, H., & Yamaguchi, M., “Analysis of multilayered CoZrNb film on-chip noise suppressor as a function of resistivity and permeability,” IEEE Magnetic letters, Volume: 7, Article: 5103904, 2016 (Chapter 3)

B. Conference presentations

[1] Ma, J., Muroga, S., Endo, Y., Hashi, S., Naoe, M., Yokoyama, H., Hayashi, Y., Ishiyama, K., “Noise suppression and crosstalk analysis of on-chip magnetic film-type noise suppressor," 2017 Magnetism and Magnetic Material, USA, CI-14, 2017

[2] Ma, J., Muroga, S., Endo, Y., Hashi, S., Yokoyama, H., Hayashi, Y., Ishiyama, K., “Analysis of magnetic film-type noise suppressor integrated on transmission lines for on-chip crosstalk evaluation,” 2017 International Symposium on Advanced Magnetic Materials and Applications, MMA-O6, Vietnam, 2017

[3] Ma, J., Aoki, H., & Yamaguchi, M., “Analysis of multilayered CoZrNb film on-chip noise suppressor as a function of resistivity and permeability,” (proceeding) IEEE International Magnetics Conference, CW-01, China, 2015

and 11 others

C. Scholarships and Awards

[1] Research fellow of Japan Society for the Promotion of Science (JSPS), Grant number 17J02041, 2015-2018

[2] Member of Program for Leading Graduate Schools, “Inter-Graduate School Doctoral Degree Program on Global Safety,” by the Ministry of Education, Culture, Sports, Science and Technology, 2015-2018

[3] Korea-Japan Joint Conference on EMT/EMC/BE, “IEEE EMC Society Japan Joint/Sendai Chapters Best Poster Award,” 2015

[4] 電気関係学会東北支部連合大会 IEEE Sendai Section Student Awards “The Best Paper Prize,” 2014

ACKNOWLEDGMENTS

After five years of great effort, I was finally able to complete this thesis. As a poor writer as I am, this part is which I conduct at the end. Many of the experiences I have got through in the past five years have allowed me to grow from an ignorant fool to a doctoral person. People standing by my side has lead me a way to understand “what is doing research,” and make me feel their enthusiasm and love when taking it as a career. Thanks for those people giving me a chance to stand on the shoulders of giants, admiring the fierce and vibrant waves of technology explosion in the frontier of world science development. Thanks for those people giving me encouragement not to give up, teaching me how to survive in difficulty, like singing loudly even in thunderstorms. Five years is not only for one Ph. D, the experience it brings to me is more valuable. The knowledge and abilities I gained during these years are important as well as the precious understanding of responsibility and ethics to be a natural person.

First I will give my greatest grateful to my research supervisor Professor Kazushi Ishiyama, who is from Research Institute of Electrical Communication (RIEC) of Tohoku University. His invaluable guidance and genuine instruction in every detail helped me doing research smoothly and efficiently. Thanks for every tip that inspired me to move the way of improvements and new challenges in my research. His expressed enthusiasm faced with academic has brought me great interesting toward scientific world and encouraged me to do well in my doctoral course.

Next I’d like to thank Professor Hideaki Sone, who is from Department of Applied Information Sciences of Tohoku University, and Professor Shin Saito, who is from Department of Electronic Engineering of Tohoku University, for their valuable advice and

recommendations.

My most sincere thanks goes to Associate Professor Yasushi Endo, who is in the Graduate School of Engineering, Tohoku University. Thanks for the valuable academic advice and taking care of me when I was in tough time; Thanks for the helping me building a more exhaustive understanding of the research word; Thanks for the care when we participated international conference abroad.

I want to give my best appreciation to my research advisor Associate Professor Shuichiro Hashi, who is from Research Institute of Electrical Communication (RIEC) of Tohoku University. Thanks him for the kind help and support to my research. He is so much capable of handling all the necessary sources, helping me establish the experiment that I have only imaged in the simulation. Without his excellent advice and every concern of my study, I could never finish these works.

I'd like to deliver my deepest gratitude to Senior Lecturer Sho Muroga, who is in the Graduate School of Engineering Science & Faculty of Engineering Science, Akita University. Thanks him for the incomparable comments about every details of my research. Thanks him for the very careful revise about every published papers and presentations of mine. His academic guidance and concern have illuminated my study way forward and encouraged me in the most difficult times. I will cherish all the e-mails and chat record in Line about all our academic discussing for those years.

I must say great thanks to Professor Masahiro Yamaguchi, who is in the Department of Electrical Engineering, Tohoku University. He was my first teacher who led me into the world of scientific research. He has showed me the spirit of a qualified scientist and taught me a logic way to do research. Additionally, I'm very grateful to Emeritus Professor Yutaka Shimada, who was in Tohoku University, for his brilliant comments and help to

my study.

I will always be grateful to Doctor Masayuki Naoe from Research Institute for Electromagnetic Materials, for his help of providing new magnetic films to my research.

Special thanks to Assistant Professor Hanae Aoki, who is in Frontier Research Institute for Interdisciplinary Sciences, Tohoku University, and Assistant Professor Ranajit Sai for their kind help and respected discussing in the first year of my doctoral course. And especially thanks them for the revise of my JSPS scholarship application, which is pretty necessary to provided me the cost of normal life to complete the Ph. D.

And there are so many kind people who gave me a hand leading me to the way of success. I'd like to express my grateful to Assistant Professor Yoshiaki Hayashi, who helped me adapt the new lab.'s life. And thanks to all my colleagues in Ishiyama's laboratory. Without them, it is impossible for me to finish my study. Thanks for their trust and collaboration. Thanks to them to give me a very nice lab study experience.

Finally, I want to extremely thank my family relatives and my friends for their supports through those years. I want to thank my mother and grandpa who always gave me love and encouragements. Thanks to my old brother who played games with me to relax. Many thanks to ChengXu and other cute friends for their care even in faraway ChengDu. Special thanks to WangYang who spends time with me to keep a good mood in daily life.

In the end, I must thank the research foundation from Japan Society for the Promotion of Science (JSPS) Research Fellow (Grant number 17J02041). And also thanks the foundation from Program for Leading Graduate Schools, "Inter-Graduate School Doctoral Degree Program on Global Safety," by the Ministry of Education, Culture, Sports, Science and Technology.

I will always cherish the great memories we made. May God bless each single of you. Thank you very much.